Biomedical Signal Processing and Control 87 (2024) 105367

Contents lists available at ScienceDirect

Biomedical Signal Processing and Control

journal homepage: www.elsevier.com/locate/bspc

Diagnosis of Community-Acquired pneumonia in children using photoplethysmography and Machine learning-based classifier

Kehkashan Kanwal [a], Syed Ghufran Khalid [b,*], Muhammad Asif [c,*], Farhana Zafar [d], Aisha Ghazal Qurashi [e]

[a] Department of Electrical Engineering, Faculty of Engineering, Science, Technology, and Management, Ziauddin University, Karachi, Pakistan
[b] Department of Engineering, Faculty of Science and Technology, Nottingham Trent University, Nottingham, United Kingdom
[c] Faculty of Computing and Applied Sciences, Sir Syed University of Engineering and Technology, Karachi, Pakistan
[d] Department of Paediatrics, Ziauddin University Karachi, Pakistan
[e] Jubilee Healthcare Centre, Coventry, United Kingdom

ARTICLE INFO

Keywords:
Photoplethysmography
Pneumonia detection
Machine learning classifier
Decision Tree
Discriminant analysis

ABSTRACT

This paper presents a novel approach for diagnosing Community-Acquired Pneumonia (CAP) in children using single-channel photoplethysmography (PPG) using machine learning Traditional diagnostic methods (x-rays systems and blood tests) for pneumonia suffer from limitations e.g., unavailability in remote rural areas, time consumption, financial burden, and reliance on invasive procedures. This novel approach uses the PPG recording alone to generate accurate and rapid diagnoses of CAP in children that may facilitate healthcare practitioners in low-resource clinical settings in future. A cross-sectional study was carried out to collect the PPG recordings of 67 paediatric participants (31 CAP and 36 healthy). Five different machine learning classifiers namely Fine Decision tree, Linear Discriminant Analysis, Weighted K Nearest Neighbour, Wide Neural Network, and Ensemble of Bagged Trees using eight PPG signal features were employed. Using weighted KNN we predicted 9 out of 10 test subjects correctly. These results demonstrate the potential of the system to improve clinical decision-making and patient outcomes since despite the thriving advancements in healthcare paediatric pneumonia remains a major health concern.

1. Introduction

The mortality rate due to paediatric pneumonia has reduced drastically in the last 20 years, however, it is still the major cause of morbidity and mortality in children especially under five years of age [1,2]. The situation is particularly alarming for middle- and lower-income countries given the prevalence of risk factors like environmental pollution, lack of immunization coverage and the rising burden on the global healthcare system especially after the COVID-19 pandemic [3,4]. According to the UN estimate, almost 5 million children die annually [5], with lower respiratory tract infections and pneumonia being the leading cause of these deaths [6]. According to WHO criteria, pneumonia for paediatric subjects under five years of age who have either cough and/or difficulty breathing with or without fever is diagnosed by the presence of tachypnoea or lower chest wall indrawing [7]. The Integrated Management of Childhood Illness (IMCI) Guidelines clearly outlines specific guidelines for the management and classification of childhood diseases like pneumonia, diarrhoea etc according to danger signs and classification of illness [8]. However, despite the widespread dissemination of standardised guidelines, many cases of pneumonia are missed and there is a need for alternative options for low-income countries [9]. Even with suspicion of pneumonia according to valid signs and symptoms on clinical grounds needs further investigation for confirmation of diagnosis so unnecessary antibiotics can be prevented when a diagnosis is more likely to be viral bronchitis that too has overlapping symptoms [10]. Severe cases of pneumonia in early childhood may give rise to complications like bronchiectasis [11] and lead to Chronic Obstructive Pulmonary Disease (COPD) in adulthood [12]. There is a variety of testing methods including blood tests and radiology-based tests along with clinical correlations by a trained medical professional that are generally employed to diagnose pneumonia, however, the aetiology for bacterial and viral pneumonia is difficult to establish in the case of paediatric patients where sputum samples are difficult to extract for culture testing [13]. Amid the rapid progress in the field of biomedical

* Corresponding authors.
E-mail addresses: kehkashan11912@zu.edu.pk (K. Kanwal), syed.khalid@ntu.ac.uk (S.G. Khalid), muasif@ssuet.edu.pk (M. Asif).

https://doi.org/10.1016/j.bspc.2023.105367
Received 11 April 2023; Received in revised form 25 July 2023; Accepted 14 August 2023
Available online 30 August 2023

signal processing and Artificial Intelligence (AI), it is both challenging and fascinating to explore new physiological signals and methods that have the potential to carry valuable information about the physiology of the respiratory system. Researchers need to strive for new diagnostic methods for paediatric pneumonia that are painless and cost-effective.

A photoplethysmography (PPG) uses an optical sensor used to detect blood volume changes. A PPG is often obtained by using a pulse oximeter which illuminates the skin and measures changes in light absorption [14]. PPG sensor has a simple design and principle to extract the signal however the PPG signal itself is complex and has a variety of components with diverse biological functions, with slight variation of sensor design and site, different applications are achieved [15]. Therefore, over the past few years, it has been extensively employed as an interesting research tool and various research objectives have been achieved by employing the technique [16]. With the strong computational power of machine learning, the possibilities of using PPG as a diagnostic tool are immense [17–19] PPG and its derivatives commonly known as velocity PPG (vPPG) and acceleration PPG (aPPG) have been found to have strong correlation with various diseases especially coronary artery diseases (CAD), Iokebe et al [20]conducted a study on aPPG for various outpatient and inpatient diseases and concluded that it contains valuable bioinformation for screening and diagnosis of many diseases other than CAD e.g., liver injury, traumas etc. Recently PPG have been employed to detect arrythmias [21], diagnosing type-2 Diabetes Mellitus (DM) [22]. Saritas et al [23] found statistically significant difference in morphology of PPG signal between control subjects, subjects with CAD with Chronic kidney disease (CKD), this making PPG a suitable non-invasive tool for diagnosing CAD in CKD patients.

Vital signs like heart rate, breathing rate, body temperature, and oxygen saturation are typically employed in clinical settings along with many blood and radiology tests to diagnose community-acquired pneumonia in both paediatric patients and adults. Also, the use of pulse oximetry is extremely common in triage units of all healthcare centres. The main idea is to have a non-invasive, fast, and low-cost point-of-care device that could assist and increase community-acquired pneumonia diagnostic accuracy by medical practitioners or healthcare professionals. In the present work, a novel attempt has been made to diagnose pneumonia using single channel PPG signal only. A cross-sectional study was performed using 31 Community-Acquired Pneumonia (CAP) participants who were admitted to the paediatric intensive care unit (PICU) at Dr Ziauddin Hospital from January 2022 to September 2022. These were compared with a control group of 36 healthy paediatric participants. To the best of our knowledge, it is the first attempt to record the PPG signal of paediatric subjects and to use the PPG signal alone to diagnose pneumonia. We extracted time and frequency domain-based features from the recorded signal. After PPG signal pre-processing and the feature extraction, five supervised machine learning classifiers were trained and tested with these PPG features to predict CAP in children among random participants.

The entire process is summarized in Fig. 1 below. The presented paper is organized as follows, in section 2 we have discussed the related work, in section 3 the methodology employed for the data collection and subsequent processes are discussed in detail. Section 4 presents the pre-processing results and training and test results for all five used classifiers, in section 5, results of data collection, pre-processing and the machine learning classifier have been discussed, and finally, in sections 6 and 7, some future directions of work has been given and the present work has been concluded.

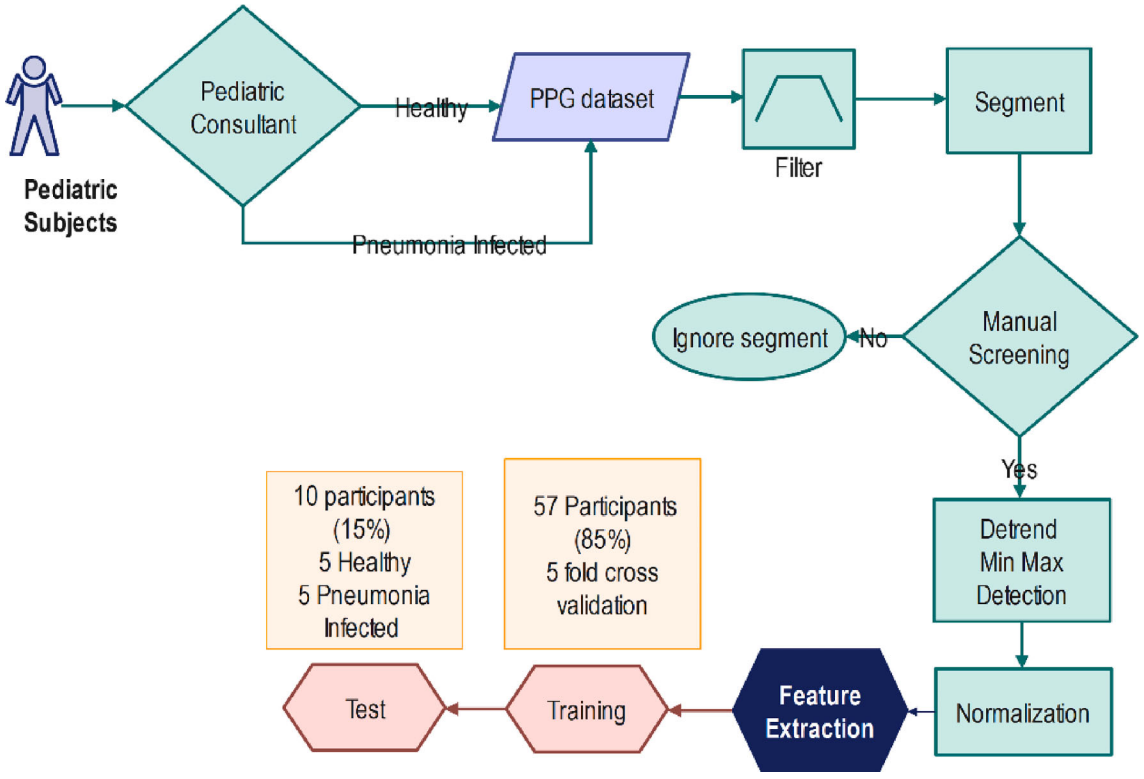

Fig. 1. Workflow for the proposed study: (a) Data collection: Photoplethysmogram of both healthy and pneumonia-infected individuals were recorded. A team of trained medical professionals under a consultant paediatrician diagnose and label the participant PPG data with PCAP or healthy tag. The PPG recordings were made using an FDA-approved oximeter connected to a host computer via a USB interface. The recordings were exported as csv files and were subsequently used in the next step; (b) Pre-processing: The PPG recordings were filtered, detrended, minimum and maximum points of the waves were marked, and locations were saved, and finally, the signal was normalized. The normalized signal was exported as csv files; (c) Features extraction: first the normalized PPG waves along with the key points detected previously were utilized to extract time and frequency domain features. The feature table with the clinician decision tag as a reference was then used to train five different machine-learning algorithms with 85% of the participants' data (57 participants) was used for training and tested with 15% participants' data (10 participants).

2. Related work

In the last few years, researchers have used chest sound as a signal of interest to diagnose and monitor respiratory disorders including pneumonia. K. Kosasih et al. Porter et al. and A. Imran et al used cough sounds for diagnosis and reported good sensitivities as [24–26]. Porter et al. used an audio recording of cough to diagnose pneumonia in restricted settings such as telehealth consultations [25]. Symptoms reported by patients (fever, acute cough, productive cough, and age) and audio files of cough were recorded and were analysed by the smartphone-based algorithm to generate a prediction for Community-Acquired Pneumonia (CAP). The proposed algorithm had high Percentage Agreement (PA) with the clinical diagnosis of pneumonia, (n = 322, positive PA [PPA] = 86.2%, negative PA [NPA] = 86.5%). H. Chen categorized wheeze, crackle, and normal respiratory sound using optimized S transform and deep residual network ResNet and obtained accuracy, sensitivity, and specificity up to 98.79%, 96.27%, and 100%, respectively [27]. E. McCollum et al. used a random-effects regression model to evaluate the association between lung sounds and radiographic pneumonia [28].

Rao et al. developed a proof-of-concept non-invasive device to identify the fluid accumulation in the lungs (consolidation), a specific characteristic of pneumonia [29]. This device, named Tabla utilized the technique of auscultatory percussion; a percussive input sound is sent through the chest and recorded with a digital stethoscope for analysis. It analyses the differences in sound transmission through the chest at audible frequencies as a marker for lung consolidation. The presented preliminary data from five pneumonia patients and eight healthy subjects demonstrated 92.3% accuracy in distinguishing between healthy subjects and patients with pneumonia after data analysis with a K-nearest neighbours' algorithm.

Another approach is to use vital signs such as respiratory rate, body temperature, heart rate etc. to monitor pneumonia. Baker et al. employed Community Health Workers (CHW) in resource-strained settings to use four different RR timers and predict pneumonia in children based on RR [30]. Four devices were evaluated and none of them performed well based on agreement with the reference standard.

W. Karlen extracted the respiratory rate using PPG, the respiratory rate gives a fair estimation since tachypnoea is an important symptom of pneumonia [31]. Capelastegui et al. suggested the use of RR along with other factors such as urea level, mental state, and blood pressure level effective enough [32]. Amirav et al. suggested that the diagnostic yield of tachypnoea among children with true bacterial pneumonia appeared to have been low, implying that it might be neither an appropriately sensitive nor a specific sign of bacterial pneumonia, thus questioning the role of this parameter in the diagnosis of pneumonia [33]. It is worth mentioning that oxygen saturation alone is not used for diagnosing Pneumonia however it is a good predictor [34]. Low oxygen saturation however could be because of reasons other than pneumonia and thus could be misleading. M. J. Lyu et al. presented the idea for the diagnosis of pneumonia using the smart dog as part of the care set-up for patients with Alzheimer's disease [35]. K. Mala et al. used three different sensors heart rate, body temperature, and respiration rate [36]. T. Salti et al. used only two sensors [37]. In a true sense, both researchers presented a mode of monitoring the relevant vital signs by medical staff rather than independently diagnosing Pneumonia. Chiu et al. described an electronic nose to detect metabolite of pneumonia in its early stages from expired gas from the patient circuit in a ventilator [38]. S. Daulou et al. described a novel Optical Biosensor (OB) using the principle of photoplethysmography to detect sepsis and severe covid-19 induced pneumonia [39]. The OB diagnosed severe COVID-19 with 83.3% sensitivity and 87.5% negative predictive value.

It is worth noting that the majority of the research targeting non-invasive methods of diagnosing pneumonia is in the prototype phase. The vital signs-based methods discussed above are in the actual sense a method of monitoring pneumonia after it has been diagnosed. After the COVID-19 pandemic, the need for remote point-of-care diagnostic tools is extremely highlighted. Therefore, finding such a tool for pediatric pneumonia is extremely important.

3. Methods

3.1. Data collection

The data for pneumonia-infected individuals was collected first from the Paediatric Intensive Care Unit (PICU) of Dr Ziauddin Hospital. The study has been approved by the Ethical Review Committee (ERC) of Ziauddin University under reference code 0140421FAENG. A team of doctors under a Paediatric Consultant diagnosed the patients with Pneumonia. The data was collected before any antiviral or antibiotic treatments were started for the subjects. In total 31 subjects were recruited in the study, 21 males and 10 females with a mean age of 2.53 years whereas the standard deviation was 4.15 years for the group. For healthy subjects, data were collected at various premises of Ziauddin Hospital and University according to the following protocol. For the healthy group we had 36 subjects, 17 of the subjects were male and 19 females. The mean age for the healthy group was 4.59 years with a standard deviation of 0.8 years. The PPG has been recorded using an FDA-approved pulse oximeter CMS 50D+, the recording software has a sampling frequency of 58.6 Hz. For each paediatric participant, a 3-minute-long PPG recording was made from right-hand fingers. We recorded other information like non-invasive blood pressure, heart rate, manual respiratory rate for one minute, and SpO_2. All the participants were in relaxed supine position and were asked to keep hand on a flat surface.

3.1.1. Inclusion and exclusion criteria

The inclusion criteria for healthy kids were as follows:

1. The subjects should not have any active infection or fever.
2. The subjects should not have any chronic condition (Diabetes, Juvenile arthritis, hypertension etc.) or genetic disorder.
3. The BMI should be normal [40].

The inclusion and exclusion criteria for subjects with pneumonia infection are as follows:

1. A team of doctors under a consultant paediatrician has confirmed pneumonia as CAP and no case of Healthcare-Associated Infection (HAI) i.e., Hospital Associated Pneumonia (HAP) and Ventilator-Associated Pneumonia (VAP) was included.
2. The subject does not have other chronic comorbid like Diabetes, Juvenile arthritis, hypertension etc.

3.2. Pre-processing

The preprocessing steps are defined below in detail, the entire process is summarized as follows in Fig. 2.

3.2.1. Segmentation

All the collected data were segmented using into a 3-second-long signal segment. The segment length was chosen to get 4–6 clear beats so that further processing steps of filter and screening of data are easier to visualize and comprehend. Eventually, for feature extraction individuals one complete beat at a time was used. The segmentation was done to remove bad-quality signal segments due to various artefacts and placement difficulties given the age of the study participants and glitches that occurred during the recording.

3.2.2. Filter selection

For the presented work, the bandpass Chebyshev 2 filter of order 12 (n = 6; number of poles) has been implemented. The cut-off frequencies for the bandpass filter have been estimated using the 256-point Fast

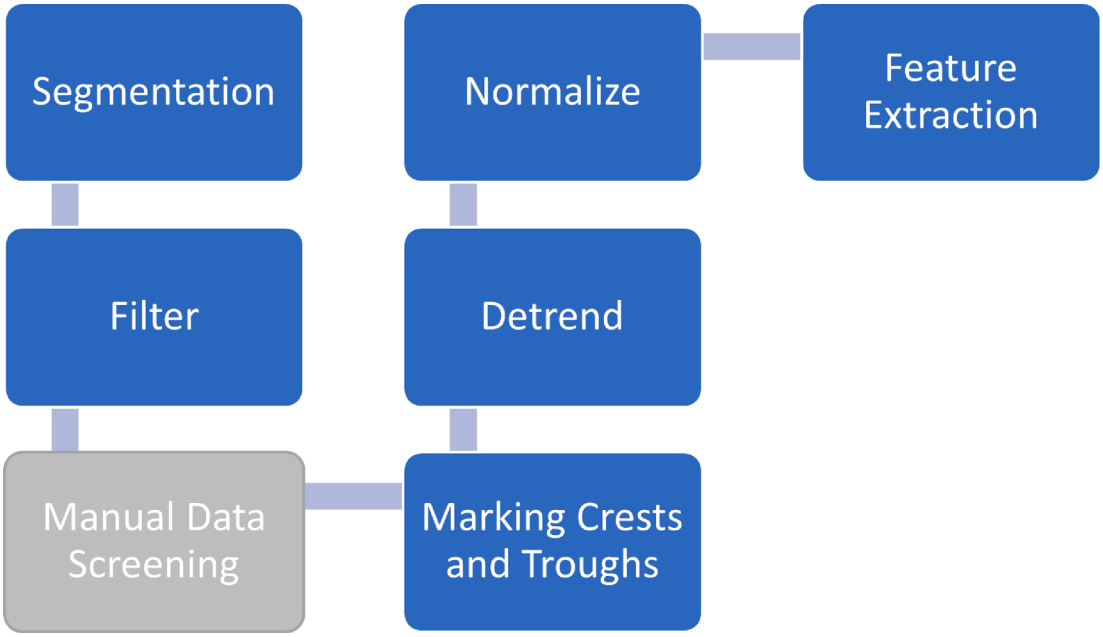

Fig. 2. Preprocessing steps employed for the presented work: the blocks in blue are performed using automated codes. The only manual expert input is needed in the data screening step exhibited in gray.

Fourier transform of the raw signal as shown in Fig. 3. The upper and lower cut off frequencies for the designed filter is 0.5 Hz to 5 Hz.

3.2.3. Data screening

The collected data was manually screened given the age group of the targeted subjects. Another code has been developed that plots each raw signal segment and filtered version, and each segment was screened and only high-quality clean data segments without electronic glitches and disturbances were saved in a different csv file. The segments were judged based on the heartbeat of the given subject and whether the overall morphology of the signal is good. The heart rate per minute of each subject was compared with beats per segment as higher beats per segment could indicate data is corrupted. Then only those PPG segments were included for subsequent steps where beat quality was excellent for diagnosis. This step has been performed similar to annotations for screening excellent quality PPG waveforms done by Elgendi [41]. This step requires manual input from expert.

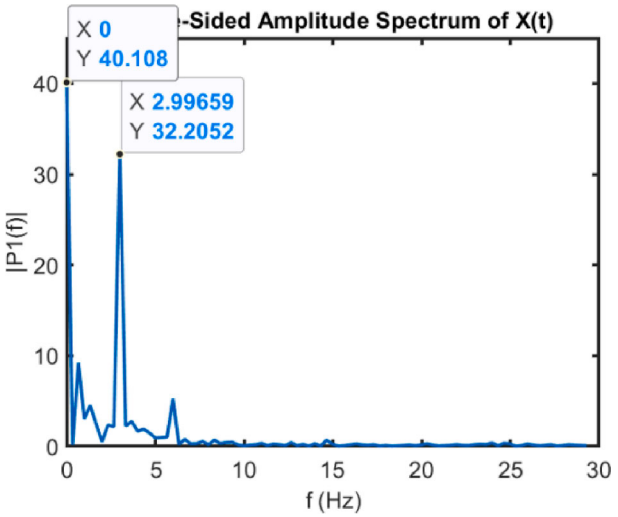

Fig. 3. Single-sided Amplitude Spectrum of the raw PPG signal as a result of taking Fast Fourier Transform (FFT) of the signal. The plot shows the main components are low frequencies below 5 Hz.

In total, approximately 4000 segments (each of three seconds) were obtained. Manual screening yielded nearly 3000 good-quality segments that were used for further processing and feature extraction. The remaining nearly 1000 segments were bad quality and not used for the current study as shown in Fig. 4. Out of 1000 bad quality segments, approximately 667 segments were from pneumonia infected participants and 333 from the healthy group.

3.2.4. Detection of crests and troughs

To extract features from the PPG signal, it is vital to detect the fiducial points in the signal so that each wave can be separated. After the manual screening, the filtered signal was used to detect and mark all relative extremum points. First order derivative test has been used for the purpose that implies that all the points where the derivative of the given PPG segment changes from positive to negative are crests, whereas it changes from negative to positive are troughs. The index position of these crests and troughs is marked, saved, and plotted.

For each given PPG segment,

$$y = f(x) \tag{1}$$

$$\frac{dy}{dx} = f'(x) \tag{2}$$

for each critical point c,f'(x) changes from negative to positive at c, then f(c) is a trough.f'(x) changes from positive to negative at c, then f(c) is a crest.

3.2.5. Detrend and normalize

After the detection of the fiducial point, the signal segments were detrended and amplitude normalization was done. The detrending was done by subtracting the best-fit line from the signal. The amplitude or y-axis normalization was done. For the normalization of each segment, we performed linear transformation on the data in a way that all the values were scales between 0 and 1.

$$x_{scaled} = \frac{x - x_{min}}{x_{max} - x_{min}} \tag{3}$$

where x_{min} = minimum value of PPG signal in each segmentand x_{max} =

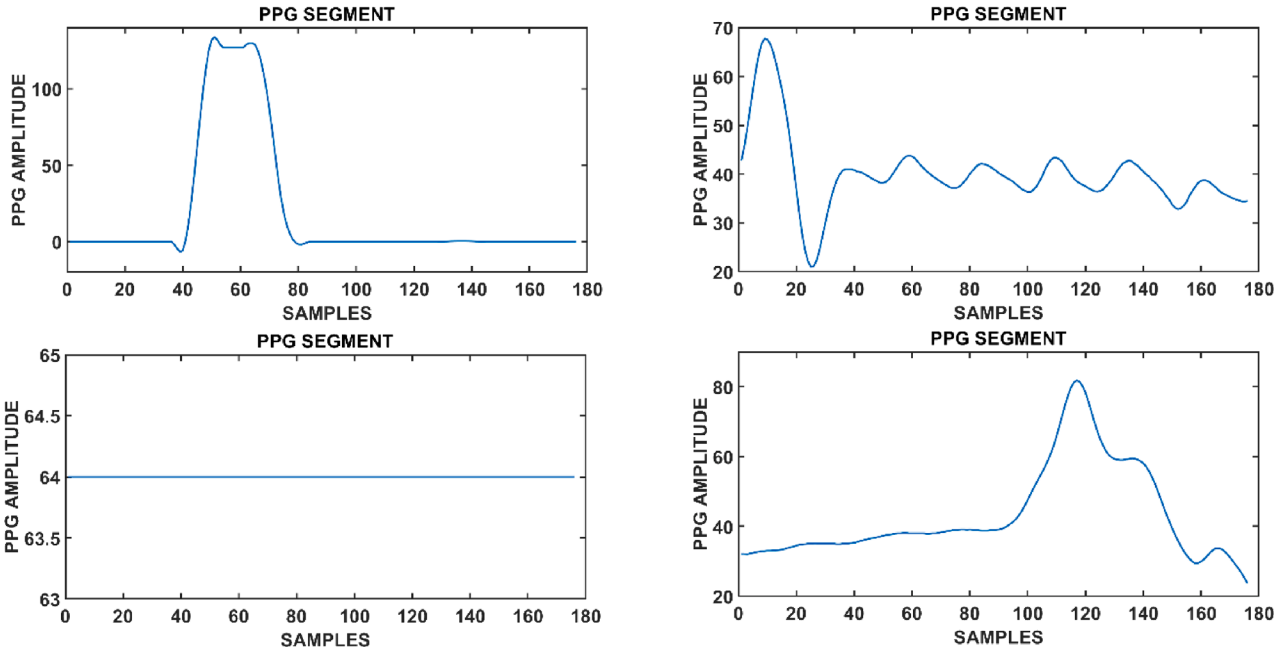

Fig. 4. Examples of bad PPG segments that were screened and discarded during the data screening process.

maximum value of PPG signal in each given segment

3.3. Feature extraction

Individual waves were extracted using the troughs. Every two consecutive points of troughs constitute one complete wave. When a single wave is extracted along with the fiducial points, all the relevant features can be extracted from it. A custom code has been implemented to perform the processing steps defined. We have extracted 8 features from each wave as shown in Fig. 5. Six features from the eight are time domain features namely, Onset, Rise time Pulse interval, $Slope_{op}$, Area, and width. The remaining two are frequency domain features namely, F_{base} and S_{Base}. These two features were extracted by taking the FFT of the waveform [42]. These are the set of features that were extracted using the key points detected on every wave in the signal. More features can be extracted after calculating the first and second derivatives of the signal, however not used for the proposed study. The features were extracted from the cleaned data of all participants separately and a feature table was made after the features were extracted to a csv file. A brief description of each feature is presented in Table 1.

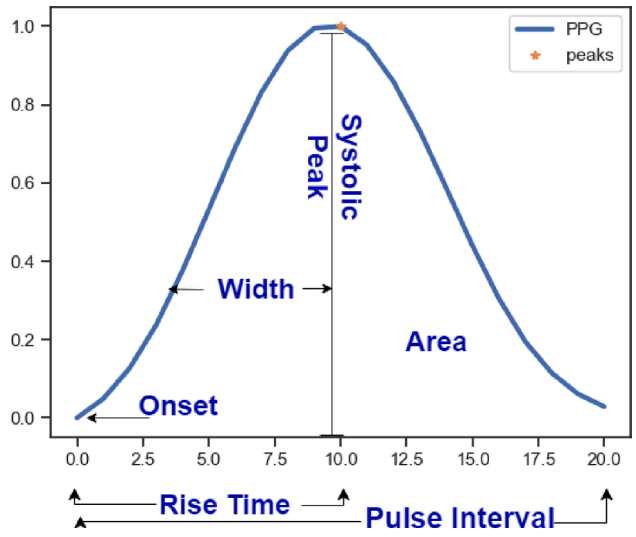

Fig. 5. Single PPG wave and the time domain features extracted from it.

3.4. Data preparation for Machine learning

For all the healthy subjects a pneumonia infection status of 0 was marked against that feature, and for the subjects with a pneumonia status of 1 was assigned. All the files were merged resulting in 411,413 feature rows. 47% (195,298 rows) features of the data belong to the healthy group and 53% (216,115 rows) features belong to subjects with pneumonia. We randomly chose 57 participants (85% of the total) for the training and remaining 10 participants (15% of the total) for the test.

3.5. Statistical analysis

Since the feature table has all eight variables containing continuous values against the dichotomous or binary outcome variable i.e., infection status. First point biserial correlation analysis was considered. Before computing the correlation coefficient, the feature table was checked for outliers and data distribution, since the point biserial correlation analysis is extremely sensitive to outliers and applies to datasets having normal distribution only [43]. For detecting outliers, box plots were made for each continuous variable as shown in Fig. 6 and the Anderson-Darling test was conducted to check for the normal distribution of the data [44]. The null hypothesis was made that the data came

Table 1
Lists the features extracted from each PPG wave. The individual waves were extracted from clean data segments of all subjects that in turn extracted the below features from each wave.

Feature Name	Description
Onset	Value of the signal at the start of each wave
Rise Time	Time is taken by the signal to attain maximum value (systolic peak)
Pulse Interval	Time is taken by the signal to complete one wave
$Slope_{op}$	The slope between onset and systolic peak
Area	The total area of the wave
Width	Width of the wave at the half-systolic peak
F_{base}	The fundamental frequency of the wave
S_{Base}	The magnitude of the fundamental component of the wave

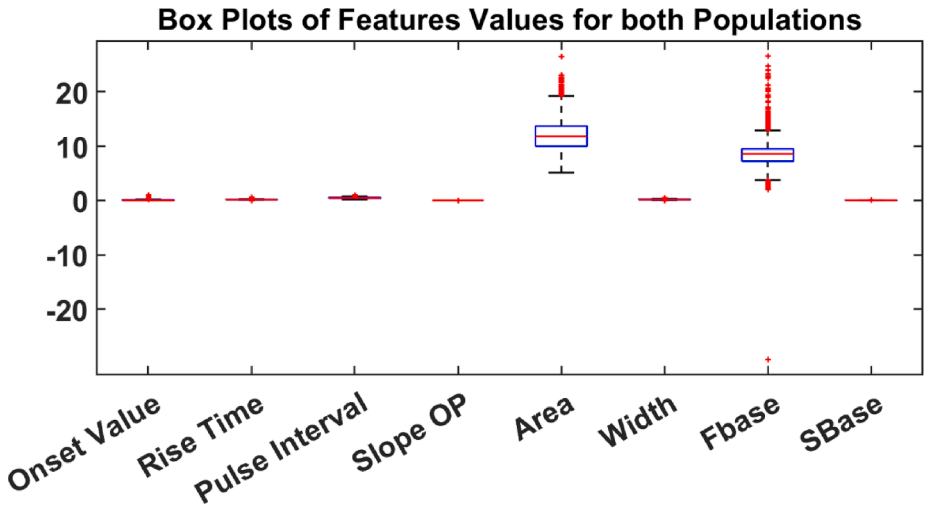

Fig. 6. Boxplots for the feature values of both healthy and pneumonia-infected individuals. It can be seen that features have a small range of values and Area and F_{base} has outliers.

from a population having a normal distribution with a 5% significance level. However, the box plots revealed outliers and the null hypothesis was rejected confirming that the data is not normally distributed. Therefore, a non-parametric test was employed to investigate the relationship between feature vectors from the healthy and pneumonia-infected individuals. We employed the Mann-Whitney *U* test or Wilcoxon rank sum test, and it confirmed that the features from healthy and pneumonia-infected individuals are different and can be used for designing a machine learning-based classifier. The test was employed because the sample size was consistent with the central limit theorem, (n_1, $n_2 \geq 30$) [45,46]. The test is also insensitive to different lengths of samples from the two populations. The null hypothesis was the features came from the same population; the alternate hypothesis was the populations are not the same with a 95% confidence interval. A two-sided test was performed, and the null hypothesis was rejected for all the variables confirming the feature values for healthy and pneumonia-infected individuals are significantly different.

3.6. Data splits

3.6.1. Random splitting of data

In order to examine the performance of the machine learning classifier with the recorded data, we trained and tested the classifier with carrying data splits by breaking the data pool into different combinations of train and test dataset randomly as follows,

1. Experiment 1: 70–30 data split
2. Experiment 2: 85–15 data split
3. Experiment 3: 90–10 data split

3.6.2. Participant based split

The data was split into 85 and 15 percent participant, 85% was used for the training and 15% was set aside for the tesst. After the classifiers have been trained, the test pool was used for testing the data. Five different classifiers have been trained and for all of them, 5-fold cross-validation has been done during the training which implies each classifier has been trained 5 times on the training data by splitting the total training data into 5 parts. Each time 4 parts were used for training and one part for validation and hence training confusion matrix and AUC-ROC curves were generated for the best results. The best classifier in each case was then used for the test with separate test data.

3.7. Machine learning classifiers

Fine Decision trees, Linear discriminant Analysis (LDA), Weighted K-Nearest Neighbour (KNN), Wide Neural Network, and Ensemble of bagged trees are the algorithms implemented for the given work. All the classifiers were trained on an i7-1065G7 CPU operating at 1.30 GHz and 1.50 GHz with 16 GB RAM and a high-performance NVIDIA processor.

3.7.1. Fine decision trees

The decision tree is one of the first algorithms to choose when the problem is binary classification. They are based on greedy algorithms that classify on a series of rules about the class properties. For the presented work, a fine decision tree was implemented. The node impurity is calculated using Gini's diversity index. If the 'D' dataset contains 'M' samples from 'c' different classes the Gini index, Gini (D) is calculated as

$$\boldsymbol{Gini}(\boldsymbol{D}) = 1 - \sum_{i=1}^{c} \boldsymbol{p}_i^2 \tag{4}$$

p_i is the relative frequency of class c in dataset D.

Since there are two classes, healthy and pneumonia infected and can be symbolised as D_1 and D_2 respectively with samples M_1 and M_2, the Gini index is,

$$\boldsymbol{Gini}_d(\boldsymbol{D}) = \frac{\boldsymbol{M}_1}{\boldsymbol{M}}\boldsymbol{Gini}(\boldsymbol{D}_1) + \frac{\boldsymbol{M}_2}{\boldsymbol{M}}\boldsymbol{Gini}(\boldsymbol{D}_2) \tag{5}$$

The maximum number of splits or depth of the tree was set to 100. The Gini index for each feature is calculated for the dataset and the root node is the feature variable with the lowest Gini. The pruning level for the constructed tree is 348. Pruning is a technique used in decision tree algorithms to reduce the complexity of the tree and prevent overfitting. Pruning involves removing certain branches or nodes from the decision tree that do not contribute significantly to the overall accuracy or performance of the tree. It implies that nodes or branches were removed till 348 depths of the tree. Fig. 7 represents the simplified process diagram for the described algorithm for our application.

3.7.2. Linear Discriminant analysis

The Linear Discriminant Analysis (LDA) algorithm uses a linear combination of predictors to predict the response variable [47]. The algorithm works by creating a new axis and projecting the data in the new axis in such a way that the distance between the mean of the classes is maximized and the variation within the class is minimized. As described in Fig. 8 below, the algorithm works by taking some feature values from each group and transforming them onto a new axis, the

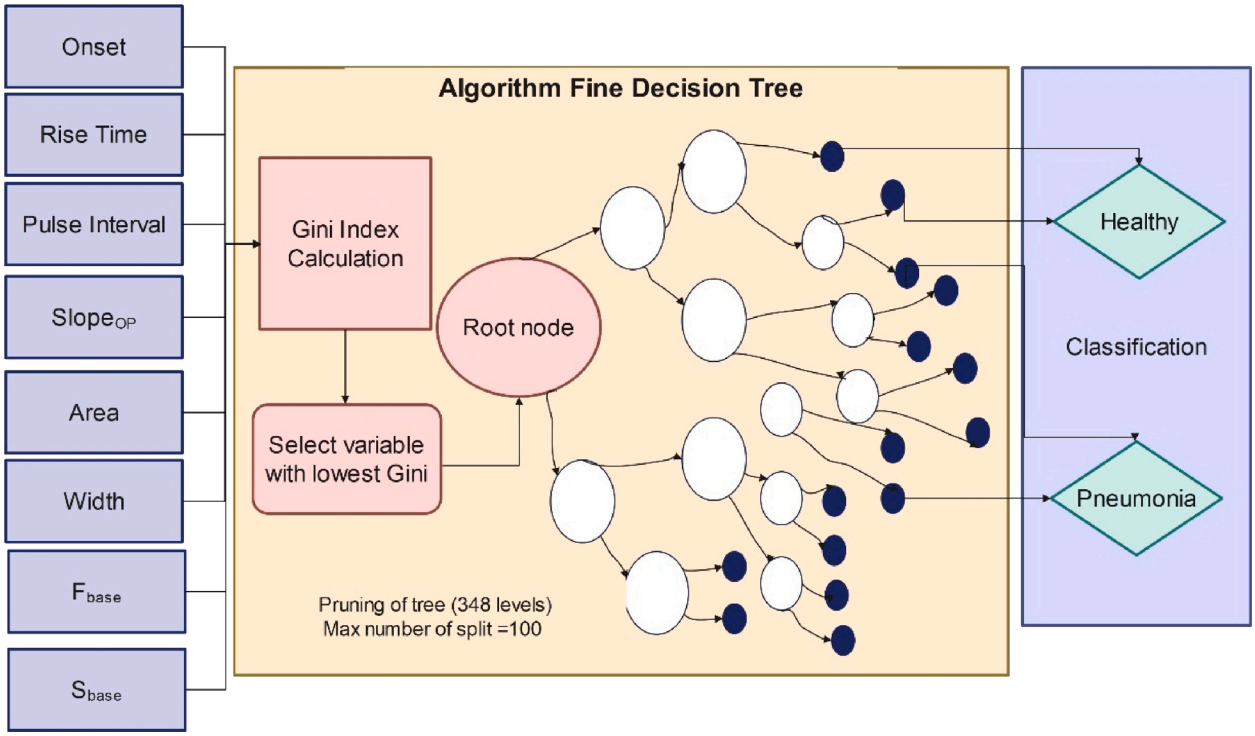

Fig. 7. Simplified flow diagram for Fine Decision Tree (DT) implemented: To the left are the eight predictors. These are the features extracted from the PPG signal. Since the data is labelled as two classes healthy and pneumonia infected, the dataset is divided into D1 and D2. The Gini diversity index for each predictor is calculated and the predictor with the lowest Gini is selected as the root node and then the tree is branched on based on branching rules. At the leaf nodes, the output is the response variable or health status. For the implemented fine tree, the maximum number of splits was set as 100. The training data is used to make the rules on which the tree is branched and constructed. The test data is used to establish the generalization capability of the formed tree.

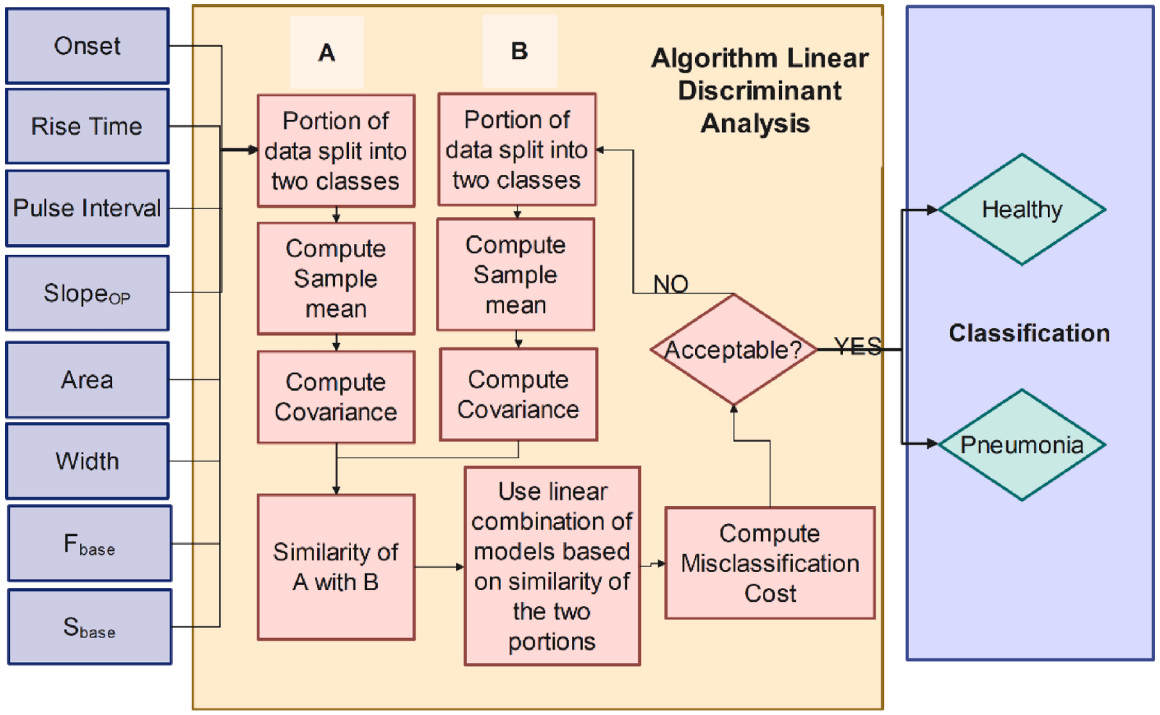

Fig. 8. Simplified flow diagram for Linear Discriminant Analysis (LDA). A predictive group discrimination model has been made using eight input features to classify them as healthy or pneumonia infected. Discriminant functions are made by selecting data points from each class and then a combination of those is used to predict the class. The misclassification cost is computed, and the model is used if the misclassification cost is acceptable. The model with maximum accuracy is used for validation and testing.

mean and covariance for each group are calculated and new points are then taken and their similarity with previously transformed data is determined. A linear combination of the models of different classes is established based on the similarity of new data with previous and then misclassification costs are calculated. If the model is acceptable, it is used for validation and then test.

3.7.3. Weighted K Nearest Neighbour

K Nearest Neighbour (KNN) algorithms are non-parametric supervised machine learning algorithms that classify the data points on basis of proximity between classes. Here a weighted KNN algorithm has been implemented that uses a weighted distance to measure the difference between the classes. Many distance matrices are employed however we have used the square inverse Euclidean distance matric. The number of neighbours was set to 10. The data were standardized first. A simplified flow diagram is presented in Fig. 9.

3.7.4. Wide Neural network

A wide neural network implies a neural network with fewer hidden layers but more neurons per layer [48]. A wide neural network has been implemented with feedforward, one fully connected layer of 100 nodes, other two layers have 10 neurons. The classifier used the ReLu activation function for the internal layer nodes and SoftMax is used with the predictor layer as shown in Fig. 10. Bayesian optimization was used for hyperparameter optimization, and the loss function is Minimal expected misclassification cost.

3.7.5. Ensemble of bagged trees

Bagging implies bootstrap aggregation, and, in an ensemble, it is meant to avoid overfitting and improve generalization [49]. In the ensemble of the bagged tree, Random Forest is bagged with a decision tree. For the implemented classifier 30 learners have been used as presented in Fig. 11.

4. Results

4.1. Data representation

Fig. 12 represents the gender distribution for the subjects included in the study. In total, 67 volunteers participated in the study. This study recruited 36 (17 males and 19 females) healthy and 31 (21 males and 10 females) pneumonia participants. After the screening, the total number of PPG waves was 411,413 observations, which were used for feature extraction. 53% (216,115 feature rows) of the data belonged to the infected group and 47% (195,298 feature rows) of the data belonged to the healthy group. Table 2 represents the age, height, and weight distribution of the two groups.

The standard deviation for age, height and weight of the healthy group is small hence the majority of the healthy individuals have age, height, and weight around the mean because it was possible to control the group parameters. The standard deviation for these parameters in pneumonia infected group is relatively high.

Table 3 represents the frequency of participants within each healthy and pneumonia infected group throughout the age range of participants included in the study. Majority of the participants in both groups are in similar age category.

4.2. Pre-processing

Fig. 13 (a) represents the raw PPG signal, and Fig. 13 (b) represents the filtered signal in blue and the detrended PPG signal in red. It can be observed that the trend line is removed. Amplitude normalization has been done so that the amplitude of the wave is between 0 and 1, it ensures the standardization of the features that are extracted consequently and the difference in the features between the two classes is not dependent on the skin properties of the subjects as shown in Fig. 13 (c). Skin pigmentation refers to quantity of melanin present in the skin which gives the skin its colour. The pigmentation has effects on light absorption and affects value of signal. However signal processing can effectively remove any such effects. Finally, in Fig. 11 (d) the crests and

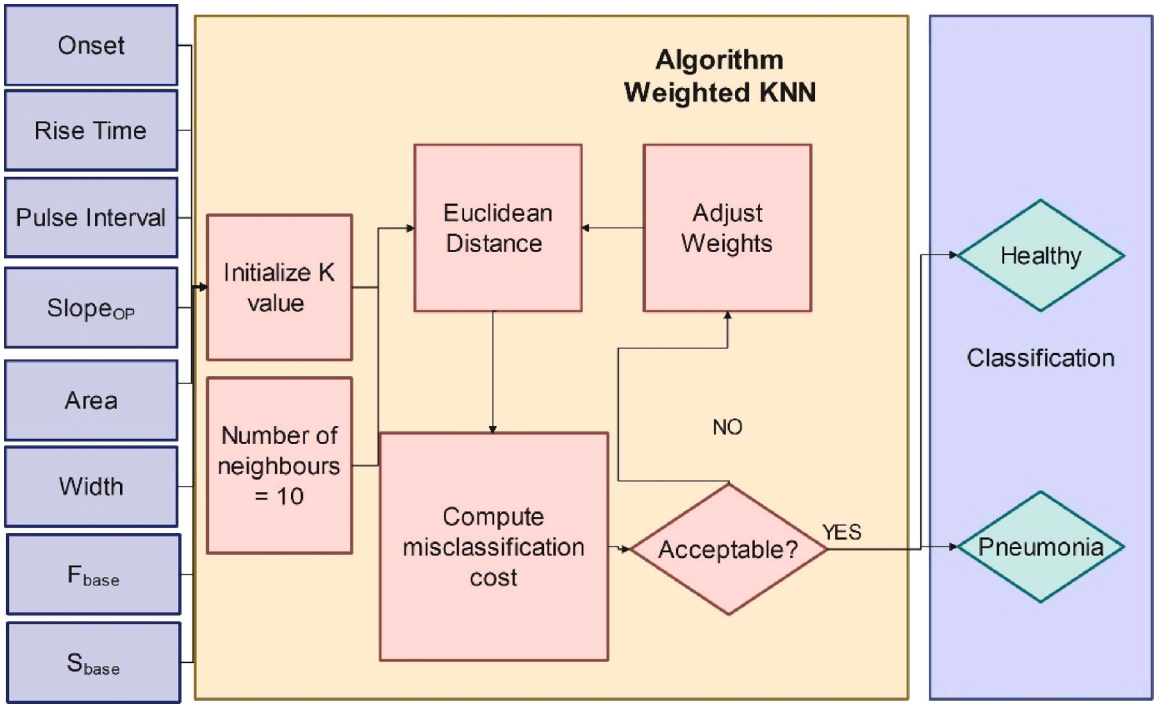

Fig. 9. A simplified process flow diagram for the weighted KNN algorithm implemented. The K value is set initially as 10 which implies that 10 neighbours will be checked for each query. For each set of training data, it works by finding the Euclidean distance between the given point with K neighbours. Then classify the data point with the most frequent class within the neighbours. The distance weights are updated if the classification accuracy is low.

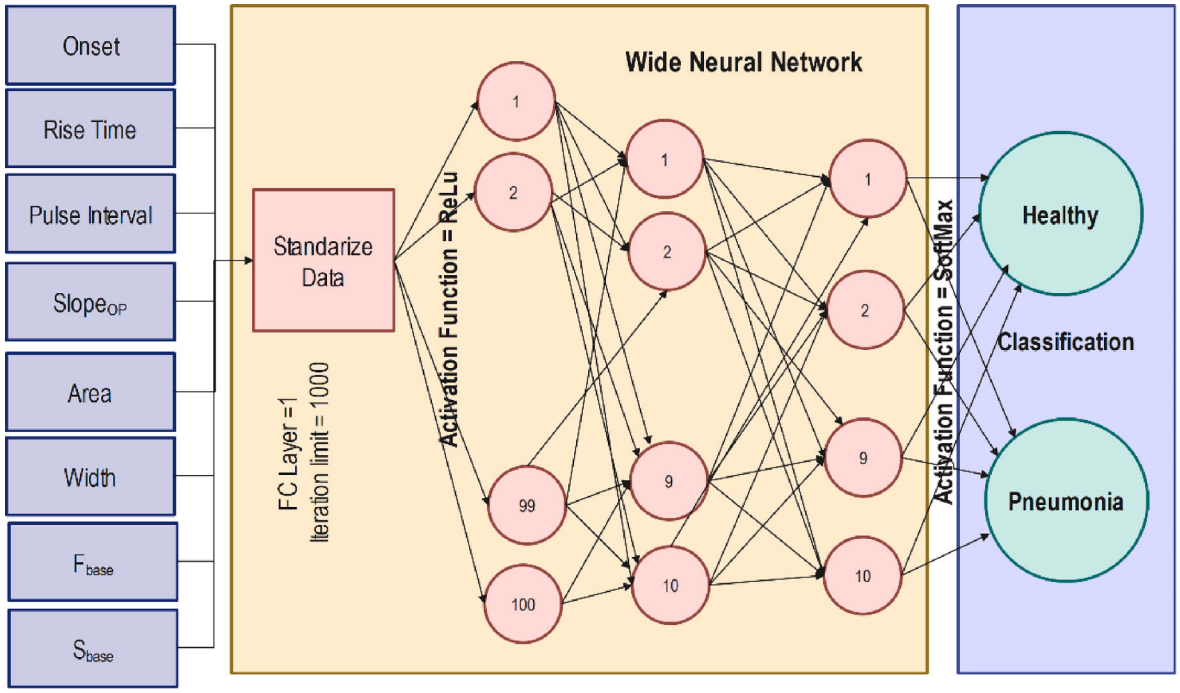

Fig. 10. Simplified flow diagram for the wide neural network. Each neuron of the first layer receives the standardized inputs. The first layer is the fully connected layer and has 100 neurons. The second- and third layers have 10 neurons each. The activation function between the layers is ReLu and the predictive layer has a SoftMax activation function. The epochs limit was set at 1000.

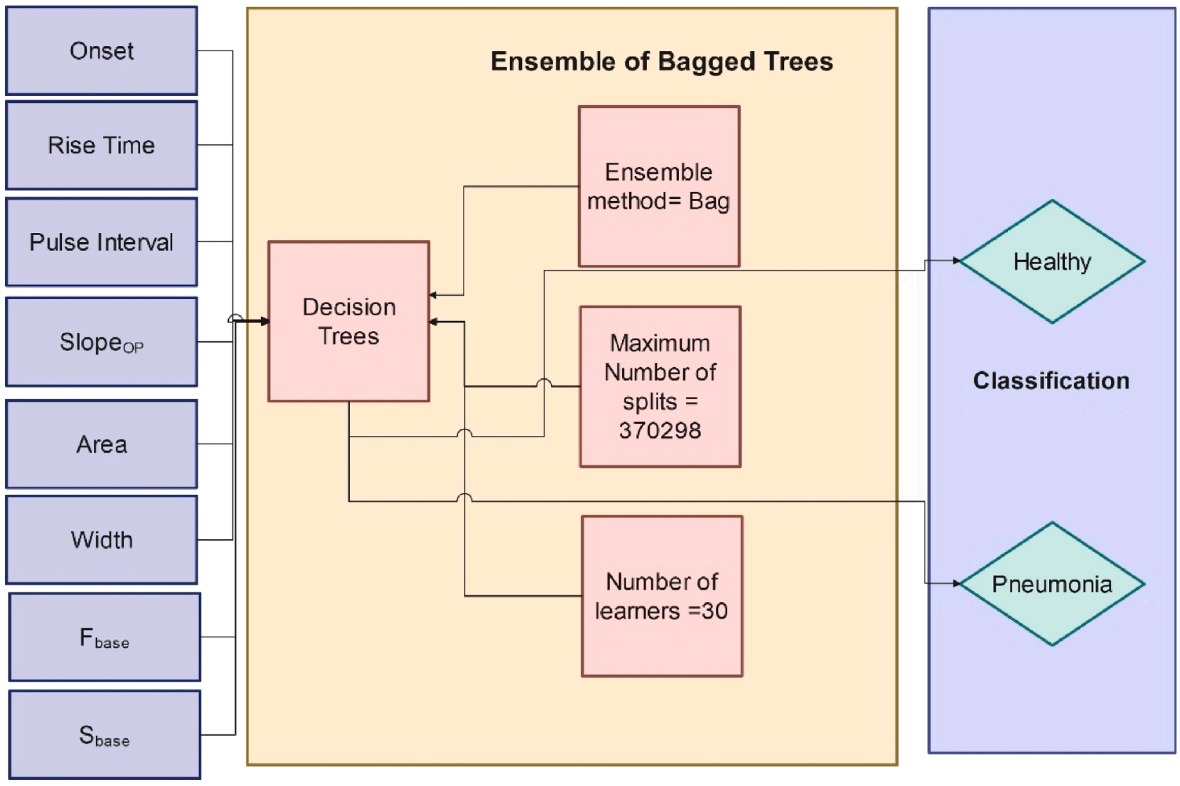

Fig. 11. Visual representation of an ensemble of bagged trees. The ensemble algorithms are based on the ideology of the wisdom of crowds. The decision-making and generalization ability of more trees is better than individual trees. The random forest is bagged with the decision trees with 30 learners. The combined trees are used to make predictions on the data.

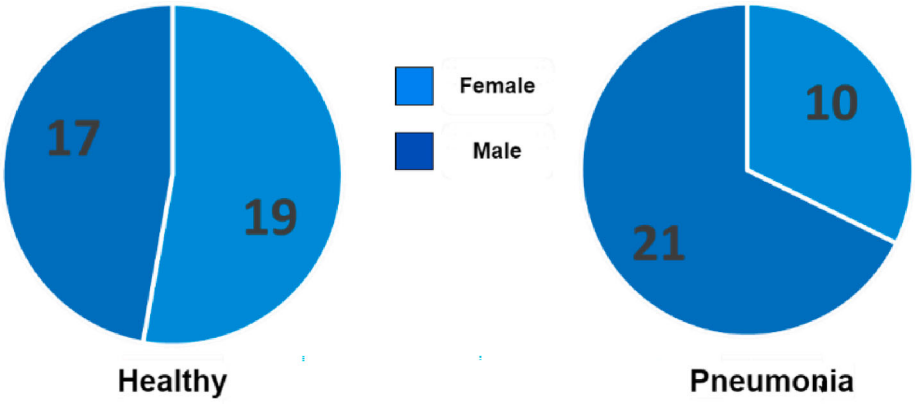

Fig. 12. Distribution of gender for subjects included in the study for both groups.

Table 2
Mean and standard deviation for age, height, and weight of the subjects included in the study.

Parameters	Healthy				Pneumonia			
	Minimum	Maximum	Mean	Standard Deviation	Minimum	Maximum	Mean	Standard Deviation
Age (Years)	3.5	6	4.6	0.8	0.2	15	2.5	4.1
Height (cm)	91	107	101.9	5.7	48	148	75.6	25.2
Weight (kg)	13	40	15.6	2.2	3	19.5	8.6	7.3

Table 3
Cross table for number of participants in each group healthy and pneumonia infected through the age range of participants included in the study.

Age	Healthy	Pneumonia
0–5 year	31	24
5–10 year	5	5
10–15 year	0	2
Total	36	31

troughs in the given segment have been marked. Each PPG wave was then extracted using the marked troughs.

4.3. Wilcoxon rank sum test

Table 4 lists the results of the non-parametric correlation test known as the Wilcoxon Rank sum test. The null hypothesis was rejected for all the feature tests confirming that the feature values from healthy and pneumonia-infected individuals differ significantly under a 95% confidence interval.

4.4. Feature selection – Minimum Redundancy maximum relevance (MRMR)

To determine distinctiveness of used features between the two classes, a feature ranking algorithm known as Minimum Redundancy Maximum Relevance (MRMR) has been used. The MRMR algorithm tends to rank individual features from a given set of features with maximum correlation with a class (or maximum relevance) and least correlation within themselves (or minimum redundance) [50]. The feature ranking using MRMR is exhibited in Fig. 14. The drop in scores between $Slope_{op}$ and S_{Base} is large and is small between rest of the features which implies importance of these features. The large drop means the algorithm is confident of selecting most important predictor.

Fig. 15 shows a plot of PPG recorded from participants of similar age from the healthy and pneumonia infected group. The plot shows the difference in pulse width, pulse interval, rise time, and the area is significant between them.

4.5. Classification with varying data splits

To ensure the classifiers built are robust, the models were trained on three different data splits apart from the one presented above as follows,

1. Experiment 1: 70–30 data split
2. Experiment 2: 85–15 data split
3. Experiment 3: 90–10 data split

Table 5 summarizes all the performance measures for all classifiers and experiments conducted on the collected data. The classifiers offer the least sensitivity of 80.26% and specificity of 71.79% with linear discriminant-based classifiers. Weighted KNN and Ensemble of Bagged Trees outclass all the classifiers for all experiments. For each experiment, in a given classifier only a slight change in performance measure ensures consistency in both validation and test results. This gives a proof of concept that using the PPG signal alone, it may be possible to diagnose pneumonia infection in paediatric patients.

4.6. Classification using participant based split

A divide of 85% and 15% was done and 57 (85% of the total participants) were kept in the training dataset, out of these 31 were from the healthy group and 26 from the pneumonia infected group. The Table 6 presents the results for test data from this participant-based split.

4.6.1. Fine decision tree

Fig. 16 represents the Decision Fine tree classifier results. The Area under the Curve (AUC) for the Receiver Operator Characteristic curve (ROC) is 0.92 for training validation and the test. The sensitivity is 86.1% and 85.2% and the specificity of 83.4% and 84.1%, for training validation and test respectively.

4.6.2. Linear Discriminant

Fig. 17 represents the linear discriminant classifier results where 75% of data has been sued for training and the rest for the test. The Area under the curve for the Receiver operator Characteristic curve is 0.83 for training validation and 0.84 for the test. The sensitivity is 80.2% and 80.3% and the specificity is 72.0% and 71.8%% for training validation

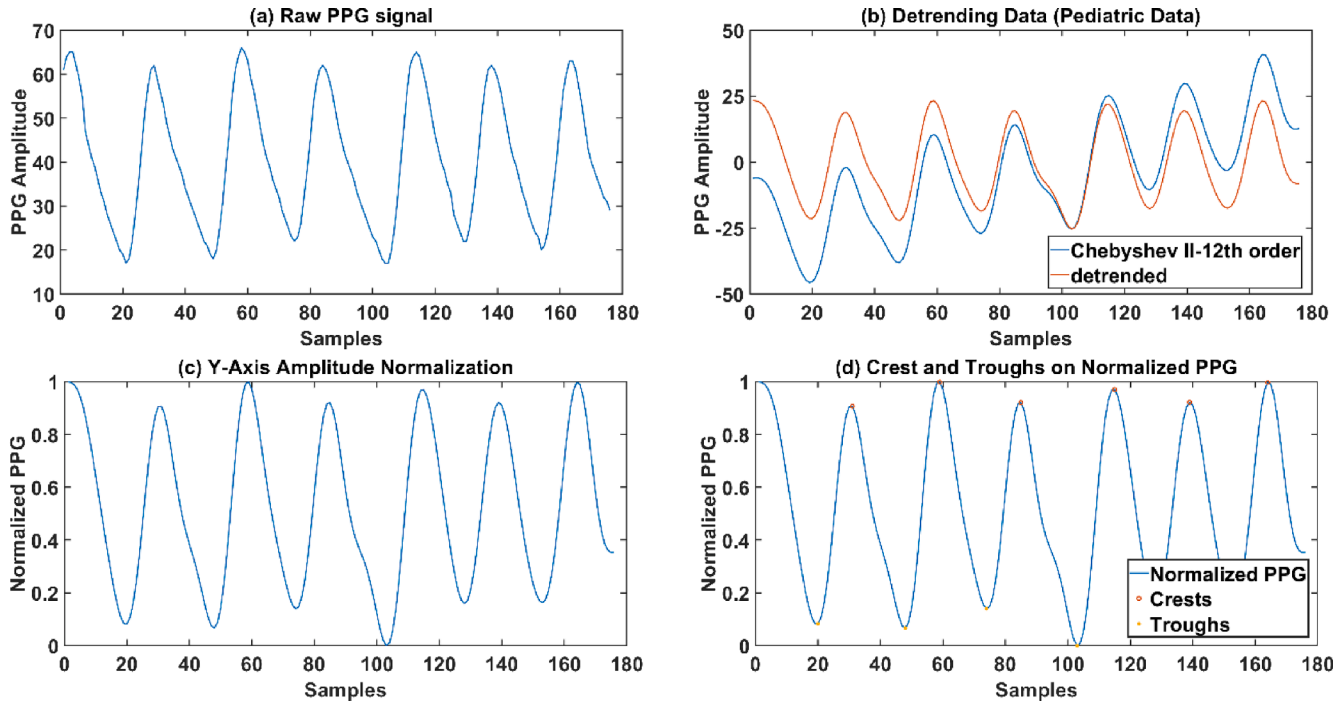

Fig. 13. Representation of detrending, normalization and detection of crests and troughs of the PPG waves in a given data segment. (a) shows the raw PPG segment (in blue), along with the detrended signal (in orange) and filtered signal (in red). (b) shows amplitude normalization of the PPG segment, and min–max normalization has been done using the minimum and maximum values of each PPG wave. (c) Each crest and trough are marked in the given segment, marking the starting and ending point of each wave along with the peak value. This has been achieved using the first derivative test.

Table 4
Results for Wilcoxon Rank Sum test: The test was performed by comparing the feature values from the healthy and pneumonia-infected individuals under a 5% significance level. The null hypothesis was the values come from the same population which was rejected for all sets of features.

Features	P value	Null Hypothesis	Z value	Rank Sum
Onset	6.1×10^{-7}	Rejected	4.99	4.03×10^{10}
Rise Time	0	Rejected	111.89	4.44×10^{10}
Pulse Interval	0	Rejected	268.37	5.04×10^{10}
$Slope_{op}$	0	Rejected	−144.58	3.47×10^{10}
Area	0	Rejected	333.01	5.28×10^{10}
Width	0	Rejected	303.49	5.17×10^{10}
F_{base}	0	Rejected	−156.28	3.42×10^{10}
S_{Base}	0	Rejected	51.78	4.21×10^{10}

and test respectively.

4.6.3. Weighted KNN

Fig. 18 represents the weighted K Nearest Neighbour (KNN) classifier results for the training and the test. The Area under the curve for the Receiver operator Characteristic curve is 0.99 and 1 for training validation and the test. The sensitivity and specificity are 100.0% for both training validation and test.

4.6.4. Wide Neural network

Fig. 19 represents the wide Neural Network classifier results for the classification. The Area under the curve for the Receiver operator Characteristic curve is 0.97 for training validation and the test. The sensitivity is 90.9% and 91.8% and the specificity is 91.0% and 92.2% for training validation and test respectively.

4.6.5. Ensemble of bagged trees

Fig. 20 represents the last classifier Ensemble of boosted trees results for the classification. The Area under the curve for the Receiver operator Characteristic curve is 1 for both training validation and the test. The sensitivity is 100.0% for training validation and the test, and the specificity is also 100.0% for both training validation and the test.

Table 7 summarizes the training time, speed, and costs for both training and testing. The wide neural network took the highest time for training, Weighted KNN had the most reasonable training time given the low-cost Ensemble of Bagged Trees has the lowest cost for the test tool. Linear discriminant was the fastest to train however with the highest training cost, it has lowest training cost but offers poor specificity.

4.7. Comparison of classification results with SpO_2

In order to diagnose these 10 patients, we used the mean values of the feature as input to each of the classifier. Fine tree predicted 7 out of 10 participants correctly giving accuracy of 70%, sensitivity of 100% and specificity of 40% only. Linear Discriminant classifier correctly predicted 8 out of 10 participants with accuracy of 80%, sensitivity and specificity of 100% and 71.43% respectively. Weighted KNN correctly predicted 9 out of 10 participants yielding 90% accuracy, 100% sensitivity and 80% specificity. Wide neural network classifier that correctly predicted 7 out of 10 participants giving accuracy of 70%, sensitivity and specificity of 80% and 60% respectively. Ensemble of bagged trees predicted 7 out of 10 patients correctly giving accuracy of 70%, sensitivity of 80% and specificity of 60%.

Table 8 compares the outcome of classification by the machine learning algorithms to the actual infection status recorded and level of SpO_2 recorded at the time of PPG data recording. It is worth noting that even with SpO_2 which can be considered within normal range, the algorithms were able to pick the infection status using the PPG features alone. This implies that SpO_2 alone might not be an accurate measure to predict pneumonia and with help of PPG signal alone accurate classification between healthy and pneumonia infected individuals is possible.

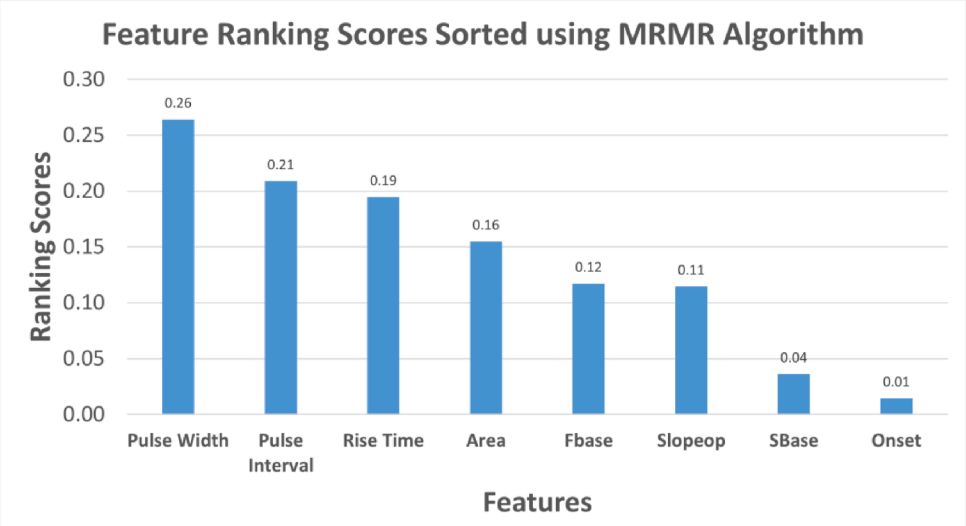

Fig. 14. Feature ranking scores using MRMR algorithm.

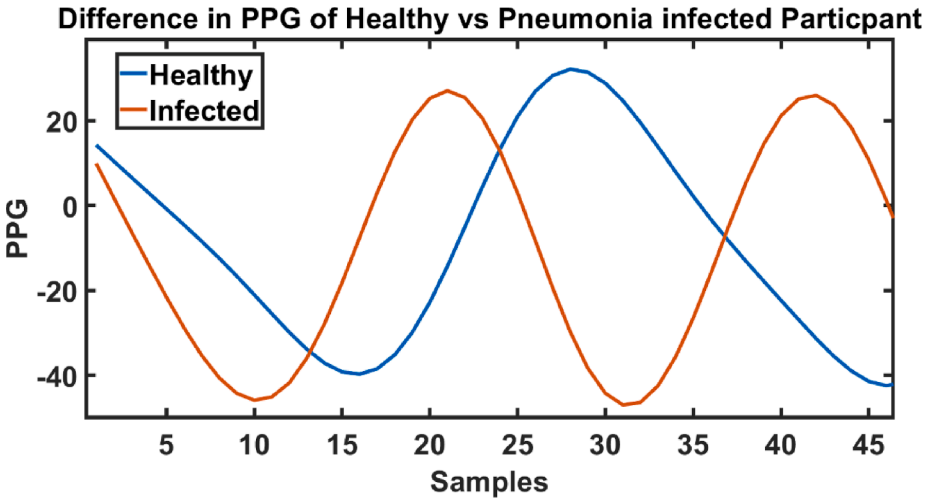

Fig. 15. The PPG recorded from individuals of healthy and pneumonia infected participants of the study. The age of both subjects is 4 years. The difference in morphology is consistent with feature ranking as exhibited by MRMR algorithm.

Table 5
Comparison of performance between the employed classifiers for the three experiments: Weighted KNN and Ensemble of Boosted trees gives the best results for all the experiments. For all the classifiers, the AUC-ROC is above 0.8, implying the classifiers can distinguish pneumonia-infected individuals from healthy subjects. The sensitivity is also high for all the classifiers, the linear discriminant has the lowest specificity.

Classifier	Experiment	Accuracy (%)	Error (%)	Sensitivity (%)	Specificity (%)	Precision (%)	F1 Score	AUC-ROC
Fine Tree	1	84.93	15.07	85.93	83.82	85.4542	0.86	0.93
	2	84.96	15.04	85.30	84.58	85.9559	0.86	0.93
	3	84.48	15.52	85.31	83.56	85.1672	0.85	0.92
Linear Discriminant	1	76.28	23.72	80.33	71.79	75.9088	0.78	0.83
	2	76.41	23.58	80.26	72.16	76.1317	0.78	0.84
	3	76.48	23.52	80.42	72.10	76.1356	0.78	0.83
Weighted KNN	1	99.99	0.00	100	99.99	100	1	1
	2	99.99	0.00	100	99.99	99.99	1	1
	3	100	0	100	100	100	1	1
Wide Neural Network	1	91.29	8.7076	91.22	91.3700	92.12	0.92	0.97
	2	91.46	8.5424	92.32	90.5191	91.33	0.92	0.97
	3	91.37	8.6258	91.27	91.4909	92.23	0.92	0.97
Ensemble Bagged Trees	1	99.99	0.0097	99.98	100	100	0.99	1
	2	99.99	0.0049	100	99.99	99.99	1	1
	3	99.99	0.0073	99.99	99.9898	99.99	0.99	1

Table 6
Comparison of performance between the employed classifiers when data has been split using Participants. The training data contains 57 participants, and the trained classifiers were tested on the remaining 10 participants data. The classifiers exhibit good sensitivity, the highest of 94% for linear discriminant and highest specificity of 69% for the weighted KNN. The highest AUC-ROC value of 0.82 is associated with Linear Discriminant classifier.

Classifier	Accuracy (%)	Error (%)	Sensitivity (%)	Specificity (%)	Precision (%)	F1 Score	AUC-ROC
Fine Tree	79.63	20.37	89.67	45.51	84.83	0.87	0.77
Linear Discriminant	84.09	15.91	94.17	49.81	86.44	0.90	0.82
Weighted KNN	77.87	22.13	80.46	69.07	89.84	0.85	0.75
Wide Neural Network	77.33	22.67	81.69	62.52	88.10	0.85	0.78
Ensemble Bagged Trees	74.37	25.63	76.29	67.85	89.10	0.82	0.79

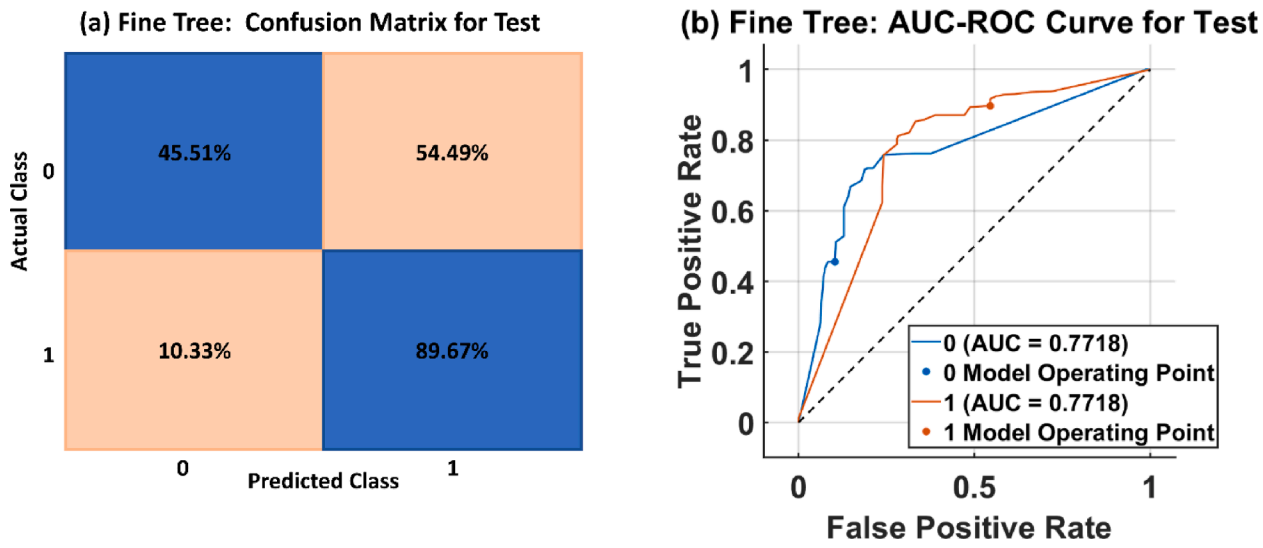

Fig. 16. Decision Tree (Fine) Classifier results when 85% of participant were used for training and 15 percent were randomly segregated and reserved for test (a) Confusion matrix for the test, and (b) AUC-ROC Curve for the test. The classifier has an AUC-ROC curve value of 0.77, specificity and sensitivity of 45.51% and 89.67% for the test respectively.

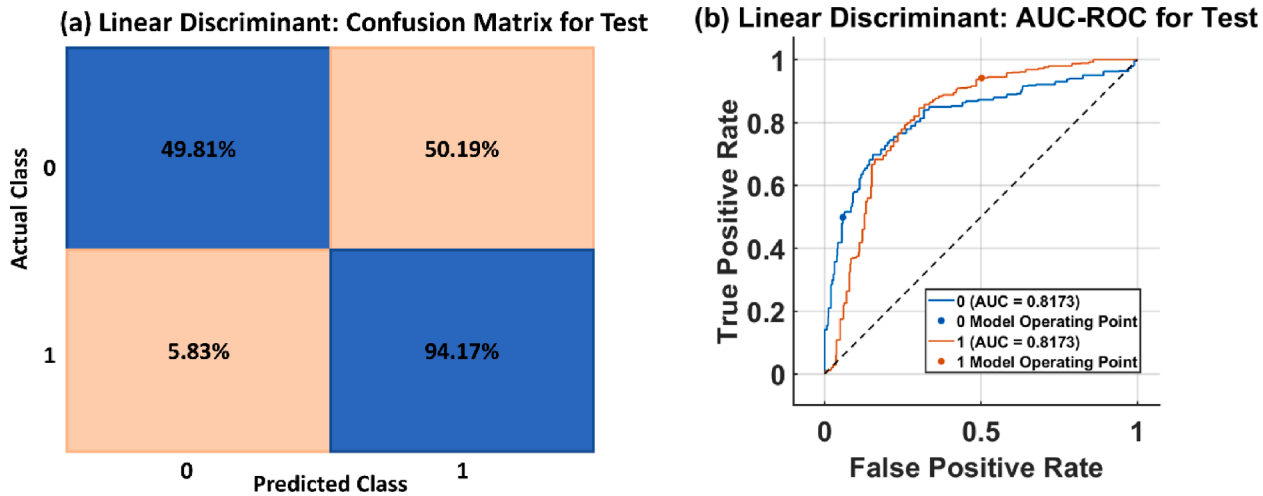

Fig. 17. Classifier results trained on the linear discriminant algorithm: when 85% of participant were used for training and 15 percent were randomly segregated and reserved for test: (a) Confusion matrix for the test, and (bb) AUC-ROC Curve for the test. The classifier has an AUC-ROC curve value of 0.82, sensitivity of 94.17% and specificity of 49.81% for the test.

5. Discussion

5.1. PPG data collection and pre-processing

The PPG dataset for the study has been acquired at Dr Ziauddin Hospital. For both groups, the number of subjects is greater than 30 so that the central limit theorem holds applicable. It was one of its kind datasets since no PPG data exist for the age group chosen (paediatrics) for the study and due to time and resource constraints the collection was stopped after the initial target of 30 patients was achieved. The data from both genders have been collected so that no gender bias is involved however the perfect balance was both impossible and irrelevant. Overall, a slightly higher number of male subjects were part of the study. The mean and standard deviation for the ages of the pneumonia-infected

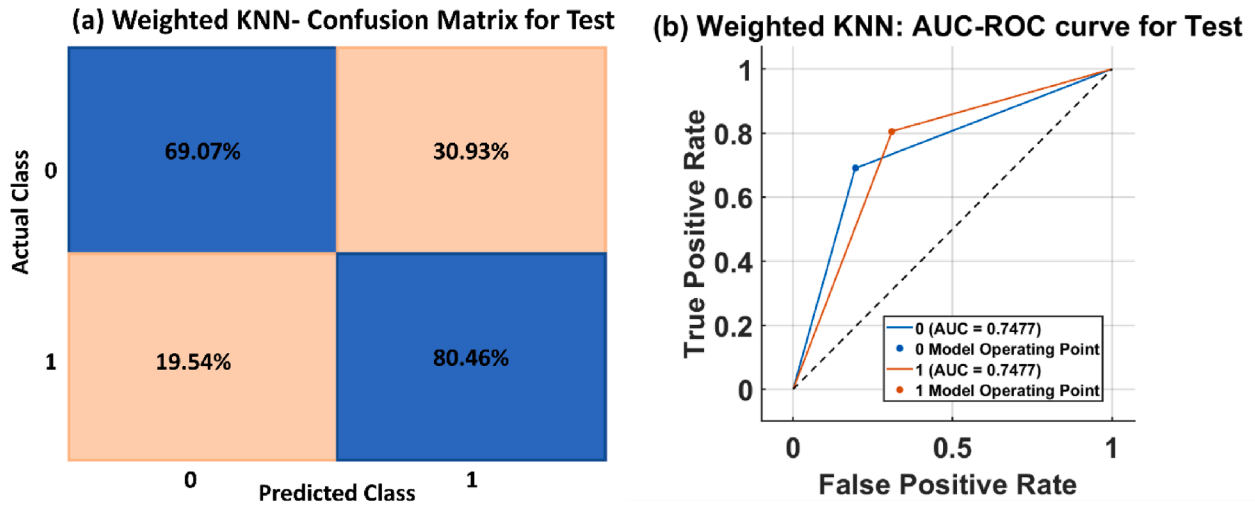

Fig. 18. Classifier results trained on weighted KNN algorithm: when 85% of participant were used for training and 15 percent were randomly segregated and reserved for (a) Confusion matrix for the test, and (b) AUC-ROC Curve for the test. The classifier has an AUC-ROC curve value 0.75 for the test, specificity of 69.07% for the test and sensitivity of 80.46%.

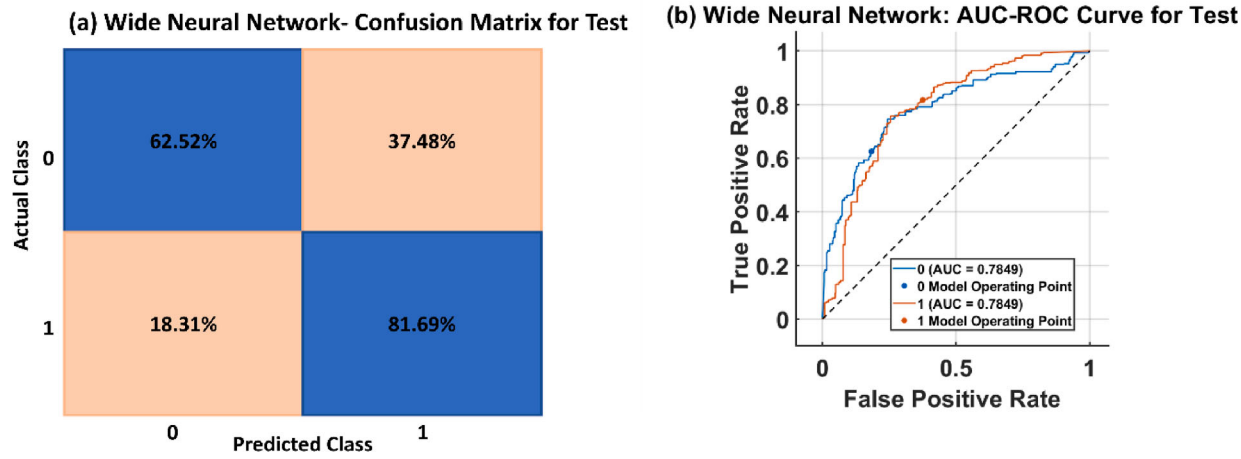

Fig. 19. Classifier based on wide Neural Network: when 85% of participant were used for training and 15 percent were randomly segregated and reserved for test: (a) Confusion matrix for the test, and (b) AUC-ROC Curve for the test. The classifier has an AUC-ROC curve value of 0.78 for the test, specificity of 62.52% and sensitivity of 81.69%% for the test.

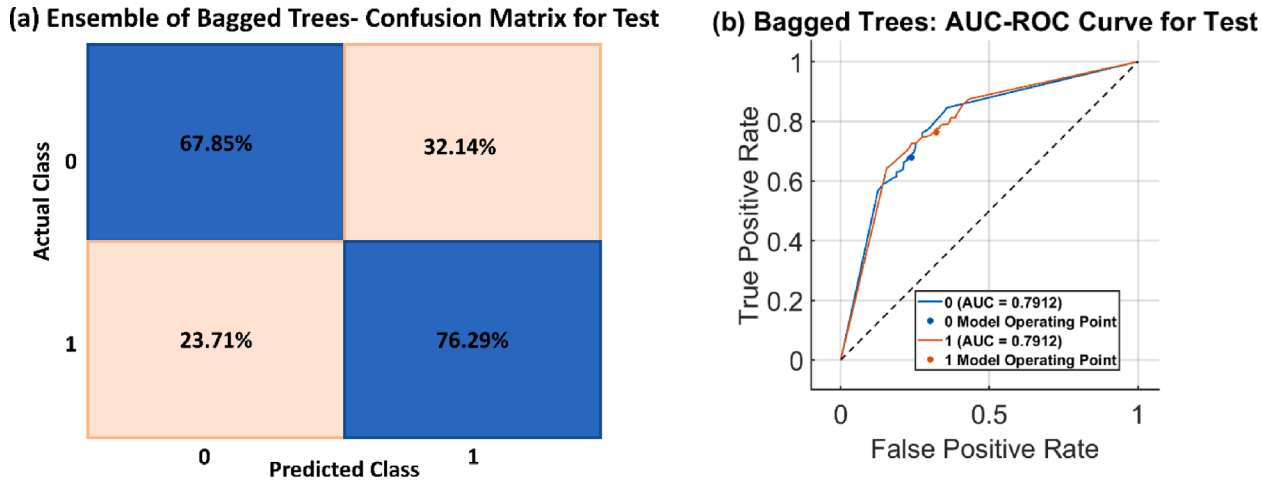

Fig. 20. Classifier based on Ensemble of Bagged Trees: when 85% of participant were used for training and 15 percent were randomly segregated and reserved for test: (a) Confusion matrix for the test, and (b) AUC-ROC Curve for the test. The classifier has an AUC-ROC curve value 0.79 for the test, specificity of 67.85 and sensitivity of 76.29% for the test.

Table 7
The training time and speed along with the total cost for training and test are presented. The weighted KNN and the linear discriminant had the least cosy. The linear discriminant classifier was the quickest to train but highest training cost. Weighted KNN and the Ensemble of bagged trees have comparable costs for training however ensemble of bagged trees took almost five times more time compared to weighted KNN. Wide Neural Network took the highest time to train.

Classifier	Training time (seconds)	Training Speed (observation/sec)	Total Cost (Training)	Total Cost (Test)
Fine Tree	59.197	880,000	36,771	4498
Linear Discriminant	24.727	610,000	63,810	3514
Weighted KNN	1117.1	4400	8	4887
Wide Neural Network	6723.3	2000	14,894	5006
Ensemble Bagged Trees	5483.9	38,000	3	5659

Table 8
Classification of 10 test participants using the five mentioned machine learning classifiers trained on 57 participants. The results of classification are compared with SpO_2 levels of each subject. The classifiers were able to predict pneumonia class even when SpO_2 levels were in the normal range. In this table the infection status of 0 is assigned to healthy participants and 1 is assigned to pneumonia infected.

Test ID	Actual Infection status	Fine tree	Linear Discriminant	Weighted KNN	Wide Neural Network	Ensemble of bagged Trees	SpO_2 (%)
1	0	0	0	0	0	0	99
2	0	1	1	0	1	1	99
3	0	1	0	0	0	0	99
4	0	1	1	1	1	1	97
5	0	0	0	0	0	0	98
6	1	1	1	1	0	1	96
7	1	1	1	1	1	1	95
8	1	1	1	1	1	1	94
9	1	1	1	1	1	1	97
10	1	1	1	1	1	0	96

individuals were not controlled because it was crucial to establish enough data. The control group however has less standard deviation for age. A similar data trend is observed for height and weight for the stated reason. The preprocessing was simple as the device used to record the signal is an accurate FDA-approved device that validates the collected data and the features which are vital for the subsequent steps. The collected data from PICU had glitches and artefacts and we systematically screened the data manually by breaking it into 3 sec long segments with an average of 4–5 beats per segment. Only the clean segments were used for feature extraction.

After the features have been extracted, the population distribution test was conducted that confirmed that the data was not normally distributed due to which non-parametric correlation analysis was conducted to establish the relationship of both population features on the infection status. It was confirmed using the Wilcoxon rank sum formula that significant variation exists between features of healthy and pneumonia-infected individuals. The PPG features extracted and then used for machine learning are primarily those that vary with heart rate and breathing rates like the Pulse interval, Area, and width of the pulse [51]. This could be a reason the algorithms were able to distinguish between the healthy and pneumonia-infected individuals because the heart rate, breathing rate, and blood pressure are known to vary [52]. However, the relationship of any PPG features with the infection status of the paediatric subject is complex, those machine learning algorithms have been used that can derive patterns from the complex relationship or dependency.

Previously, Rao et al also used [53] the machine learning algorithm KNN with chest sounds to diagnose respiratory anomalies. Kosasih et al. [24] used logistic regression on the feature extracted from cough and achieved 94% and 63% sensitivity and specificity respectively with the combination of wavelets with features the results improved. To summarize this attempt is the first to detect a specific pathology i.e., childhood pneumonia by employing PPG as a signal of interest and applying machine learning to the PPG features. K. Mala [36] proposed a sensor-

Table 9
Comparison of proposed study with previously done similar work.

Authors	Signal used	Methodology	Features	Number of subjects
A Rao (2018)	Chest sound	KNN	MFCC, Spectral centroid	5 Pneumonia, 8 Healthy
K Kosasih (2015)	Cough sound	Logistic regression	Mel Cepstral coefficients, non-Gaussian index	91 subjects, 815 cough sounds
K Mala (2016)	Vital signs	Dashboard on mobile phone, the data values are sent for remote monitoring	RR, HR, SpO_2, temperature	3 subjects (2 adults, one child)
T Salti (2019)	Vital signs	Data transmission from sensors to a mobile app via Bluetooth	RR, SpO_2	9 human subjects
P Porter (2021)	Cough sound	Logistic regression	Patient symptoms, cough sound	322 subjects
A. Imran (2020)	Cough Sound	Cloud-based AI Engine to Predict COVID-19	Mel spectrogram	ESC-50 dataset
H Chen (2019)	Respiratory Sound	Optimized S Transform (OST) on ResNet	Spectrogram of OST	Int. Conf. on Biomedical Health Informatics (ICBHI) Scientific challenge database
ED McCollum (2020)	Chest Sound	*t*-test, fisher exact test	Odd Ratio for (Normal vs radiographic pneumonia), (mortality vs alive) and (abnormal vs normal	792 enrolled paediatric subjects (PERCH)
Proposed Study	PPG	Machine learning classifiers (Fine Decision Tree, Linear Discriminant Analysis, Weighted KNN, Wide Neural Network, and Ensemble of Bagged Trees)	Six-time domain features (Onset, Rise time, Pulse interval, $Slope_{op}$, Area, Width) and two frequency domain features (F_{base}, S_{base})	31 pediatric pneumonia, 36 healthy pediatric subjects

based wearable diagnostic and monitoring device to monitor the vital signs of patients with pneumonia. This research was more inclined towards the cost feasibility and practicality of the design instead of the sensitivity and specificity of diagnosing pneumonia. Salti et al. [37] also proposed a device based on vital signs and showed a 70% and 90% correlation with oxygen saturation and respiratory rate data respectively. A summary of comparison of previous work and proposed study is presented in Table 9.

5.2. Machine learning classifiers

We have implemented five different machine learning classifiers to check the consistency of the concept that the PPG signal alone using the extracted features can be used to predict the infection or health status of pediatric subjects. The following five classifiers were used because they are straightforward and easier to implement, also they are robust and tend to avoid overfitting and work well even with fewer data. These classifiers also have the potential to be used in real-time applications.

First Fine decision trees were selected because of their high flexibility and easy interpretability and have been employed actively for binary classification problems using PPG and other biological signals for similar applications [54].

Linear Discriminant Analysis was also chosen given it is fast, accurate and easy to interpret and the problem to solve is a classic binary classification where data is divided into two distinct classes. These classifiers are frequently used with PPG-based applications [55].

K nearest Neighbour was employed because they give highly accurate results however, they are hard to interpret and have memory usage since all the data has been trained on a GPU-accelerated system, the memory usage was not a concern. Also, KNN is a lazy algorithm, the results may vary if new data is introduced in future. This limits the scope of accuracy for the study. However, KNN-based classifiers are excellent candidates for binary classification problems using PPG signals [56].

Neural networks have been an excellent candidate for complex patterns of relationship between features and outcomes, they have been used with PPG signals for both regression and classification problems [57] therefore attempt has been made to utilize a wide neural network for the proposed study and accuracy above 70% was obtained with high specificity and sensitivity of above 60%.

The Ensemble classifier is generally expected to outclass all the other individual classifiers and hence used as a comparison to get the maximum performance; however we could not achieve the desired specificity. Here the ensemble of bagged trees has attempted to utilize the prediction capability of a pool of multiple intelligent trees to reduce the generalization error offered by each classifier. They are employed with various input signals for a variety of applications [58–60].

For the given data, the weighted KNN outperformed all the classifiers with maximum accuracy, sensitivity, and specificity with the lowest error. The wide neural network also exhibited promising results with accuracy above 77% and further optimization and fine-tuning of parameters can be done to improve the results using a wide neural network however it takes the most time to train given its complex nature. The fine decision tree though very complex to interpret the given number of predictors has a high error rate of 20% however the AUC is acceptable. The least successful classifier is linear discriminant, it offers excellent sensitivity with poor specificity, since the relationship of the response variable (health status) may not be related to the linear combination of predictors used for the study.

6. Study limitations

This research is only using PPG signal as input and based on features extracted from the signal, machine learning classifiers have been trained that are discussed below. The attempt to diagnose or screen from pneumonia using chest sounds is undoubtably the most common practice. The digitized stethoscope that could pick chest sounds is also a promising tool as reported in literature as discussed above in section 5.1. The abnormal chest sounds are a characteristic feature in variety of disorders like asthma, COPDs, upper and lower respiratory infections such as pneumonia. The sound-based methods can be more specific and deterministic for differentiating these diseases among the unhealthy subjects.

The current study since focused on single sensor input, doesn't take into account the effects of cough or any abnormal chest sounds. To study the effects of cough on PPG, one would need an annotated dataset of PPG with respect to coughing episode. During the PPG data collection, we would need to note the start and end of cough episode and mark this on PPG waveform to study these effects. We have not annotated the PPG dataset presented in this study.

The focus of this study is to distinguish Pneumonia and healthy participants from PPG signal only. Therefore, only pneumonia participants were recruited for the presented study against healthy volunteers to evaluate the performance of supervised machine learning algorithm. If we include participants, in order to train the algorithms from multiple groups of illnesses e.g., influenza, COVID-19 and pneumonia, more participant would be needed to differentiate among the clusters.

7. Future directions

This study reports the first-of-its-kind dataset of PPG recordings for paediatric subjects. Since the general morphology of the PPG signal varies considerably with age, this dataset could help test different algorithms established already for applications discussed above for adults. This study established the possibility of diagnosing respiratory tract pathologies using the PPG signal alone because this signal is known to carry valuable information regarding respiratory and cardiovascular systems [61].

The research presents a novel concept of diagnosing paediatric pneumonia using PPG however there are certain limitations of the current work. Due to resource constraints, no follow-up data collection could be performed. However, to have such a system in form of a medical device, it is important to have a large-scale prospective and longitudinal study on both the control and pneumonia-affected subjects. It is also worth assessing if differences in PPG features exist within subgroups of paediatric patients based on their ages, i.e., would we have more stable and consistent models if we separate infants from older paediatric patients? Currently, we have not included any adults in the study, but it has been estimated that the algorithm for adults can be very different from those for paediatric subjects. We intend to use more classifiers for participant based split and intend to explore better ways to use the features instead of their mean values as input to obtain better prediction results. In future, we intend to implement the system on GPU-based standalone controllers e.g., Jetson Nano [62,63]. It is also recommended that following the large-scale longitudinal study, the algorithms go through clinical trials.

In future, using more sensors and physiological parameters, the PPG dataset can be annotated to include effects of abnormal chest sounds and cough on PPG. More group of participants suffering from diseases other than pneumonia can be collected to test the specificity of PPG in each disease.

8. Conclusion

Paediatric pneumonia remains one of the deadliest diseases for children across the globe. It is a fact that early screening for pneumonia with the painless and cost-effective point-of-care diagnostic tool can be vital in making an accurate diagnosis and providing proactive treatment which may decrease the mortality rate and help avoid complications as a consequence of severe disease. The findings of this study suggest that single-channel PPG could be one such tool. For the presented work a cross-sectional study was performed as a proof of concept. PPG data has been collected for paediatric subjects which to the best of our knowledge

was never collected before [64–66]. With the collected data, it is safe to conclude that weighted KNN and an ensemble of bagged trees are the best classifiers to differentiate between the healthy and pneumonia-infected subjects. Although PPG has been an established signal of greater interest for many applications including BP estimation [67,68], glucose [22,69] and cholesterol level estimation [70,71], sleep apnoea detection [72,73], arrhythmia detection [74], etc., it is vital to point out that no such attempt of screening the subjects have been made so far for lower respiratory tract infection or pneumonia.

CRediT authorship contribution statement

Kehkashan Kanwal: Conceptualization, Methodology, Software, Validation, Formal analysis, Investigation, Data curation, Visualization, Writing – original draft. **Syed Ghufran Khalid:** Conceptualization, Methodology, Validation, Formal analysis, Supervision, Writing – review & editing. **Muhammad Asif:** Validation, Writing – review & editing, Supervision, Project administration. **Farhana Zafar:** Project administration, Resources, Data curation. **Aisha Ghazal Qurashi:** Data curation, Writing – review & editing.

Declaration of Competing Interest

The authors declare the following financial interests/personal relationships which may be considered as potential competing interests: [Kehkashan Kanwal has PhD fellowship from Higher Education Commission Pakistan under HEC Indigenous 5000 PhD fellowship program (Pin number: 518–74863-2EG5-064)].

Data availability

The authors do not have permission to share data.

Acknowledgement

The authors would like to express their deepest gratitude to the staff of the OPD triage and Paediatric Intensive Care Unit (PICU) of Dr Ziauddin Hospital; Miss Shama, Mr Khurram Pervaiz (PICU Ward Incharge), Mr Amir Yousuf and Mr Alam Sher (Technicians) for their volunteering and constant support during the data collection phase. K. Kanwal would like to thank Ms Iqra, Dr Saad Abdullah, Dr Saad Jawaid Khan, Dr Bilal Ahmad Usmani, and Muhammad Rizwan for their valuable support and suggestions throughout the work.K. Kanwal would like to express deepest gratitude to Higher Education Commission Pakistan for PhD studentship under HEC Indigenous 5000 PhD fellowship program (Pin number: 518–74863-2EG5-064).

References

[1] D. Marangu, H.J. Zar, Childhood pneumonia in low-and-middle-income countries: An update, Paediatr. Respir. Rev. 32 (Nov. 2019) 3–9, https://doi.org/10.1016/J.PRRV.2019.06.001.
[2] "Every child's right to survive: An agenda to end pneumonia deaths - UNICEF DATA." https://data.unicef.org/resources/every-childs-right-to-survive-an-agenda-to-end-pneumonia-deaths/ (accessed Feb. 17, 2023).
[3] O. Karlsson, R. Kim, A. Hasman, S.V. Subramanian, Age distribution of all-cause mortality among children younger than 5 years in low- and middle-income countries, JAMA Netw. Open 5 (5) (May 2022) e2212692–e, https://doi.org/10.1001/JAMANETWORKOPEN.2022.12692.
[4] D. Goodman, et al., Challenges in the diagnosis of paediatric pneumonia in intervention field trials: recommendations from a pneumonia field trial working group, Lancet Respir. Med. 7 (12) (Dec. 2019) 1068–1083, https://doi.org/10.1016/S2213-2600(19)30249-8.
[5] "CME Info - Child Mortality Estimates." https://childmortality.org/data (accessed Feb. 17, 2023).
[6] C. Troeger, et al., Estimates of the global, regional, and national morbidity, mortality, and aetiologies of lower respiratory tract infections in 195 countries: a systematic analysis for the Global Burden of Disease Study 2015, Lancet Infect. Dis. 17 (11) (Nov. 2017) 1133–1161, https://doi.org/10.1016/S1473-3099(17)30396-1.
[7] "Pneumonia in children." https://www.who.int/news-room/fact-sheets/detail/pneumonia (accessed Apr. 04, 2023).
[8] S. Gove, "Integrated management of childhood illness by outpatient health workers: technical basis and overview. The WHO Working Group on Guidelines for Integrated Management of the Sick Child.," *Bull World Health Organ*, vol. 75, no. Suppl 1, p. 7, 1997, Accessed: Apr. 04, 2023. [Online]. Available: /pmc/articles/PMC2486995/?report=abstract.
[9] O.T. Uwemedimo, T.P. Lewis, E.A. Essien, G.J. Chan, H. Nsona, M.E. Kruk, H. H. Leslie, Distribution and determinants of pneumonia diagnosis using Integrated Management of Childhood Illness guidelines: a nationally representative study in Malawi, BMJ Glob. Health 3 (2) (2018) e000506.
[10] A. Singh, A. Avula, and E. Zahn, "Acute Bronchitis," *StatPearls*, Feb. 2023, Accessed: Apr. 04, 2023. [Online]. Available: https://www.ncbi.nlm.nih.gov/books/NBK448067/.
[11] A. Kumar, R. Lodha, P. Kumar, S.K. Kabra, Non-cystic fibrosis bronchiectasis in children: Clinical profile, etiology and outcome, Indian Pediatr. 52 (1) (Jan. 2015) 35–37, https://doi.org/10.1007/S13312-015-0563-8/METRICS.
[12] A.B. Chang, C.A. Byrnes, M.L. Everard, Diagnosing and preventing chronic suppurative lung disease (CSLD) and bronchiectasis, Paediatr. Respir. Rev. 12 (2) (Jun. 2011) 97–103, https://doi.org/10.1016/J.PRRV.2010.10.008.
[13] L. Moreno, J.A. Krishnan, P. Duran, F. Ferrero, Development and validation of a clinical prediction rule to distinguish bacterial from viral pneumonia in children, Pediatr. Pulmonol. 41 (4) (Apr. 2006) 331–337, https://doi.org/10.1002/PPUL.20364.
[14] K. Shelley, S. Shelley, Pulse Oximeter Waveform: Photoelectric Plethysmography [Online].Available: Clinical Monitoring: Practical Applications for Anesthesia and Critical Care no. May (2001) 420–423 https://www.researchgate.net/profile/Kirk_Shelley/publication/224765089_Pulse_Oximeter_Waveform_Photoelectric_Plethysmography/links/0c960529365c4977a4000000.pdf.
[15] P.A. Kyriacou, S. Powell, R.M. Langford, D.P. Jones, Esophageal pulse oximetry utilizing reflectance photoplethysmography, I.E.E.E. Transactions on Bio-Medical Engineering 49 (11) (Nov. 2002) 1360–1368, https://doi.org/10.1109/TBME.2002.804584.
[16] C. El-Hajj, P.A. Kyriacou, Deep learning models for cuffless blood pressure monitoring from PPG signals using attention mechanism, Biomed. Signal Process. Control 65 (Mar. 2021) 102301, https://doi.org/10.1016/J.BSPC.2020.102301.
[17] J. Zhang *et al.*, "Diagnostic Features and Potential Applications of PPG Signal in Healthcare: A Systematic Review," *Healthcare 2022, Vol. 10, Page 547*, vol. 10, no. 3, p. 547, Mar. 2022, 10.3390/HEALTHCARE10030547.
[18] J. Park, H.S. Seok, S.S. Kim, H. Shin, Photoplethysmogram analysis and applications: An integrative review, Front. Physiol. 12 (2022) 2511, https://doi.org/10.3389/FPHYS.2021.808451/BIBTEX.
[19] C. El-Hajj, P.A. Kyriacou, A review of machine learning techniques in photoplethysmography for the non-invasive cuff-less measurement of blood pressure, Biomed. Signal Process. Control 58 (2020) 101870, https://doi.org/10.1016/J.BSPC.2020.101870.
[20] T. Iokibe, M. Kurihara, Y. Maniwa, S. Ohta, I. Uchida, M. Amata, M. Yamamoto, Chaos-based quantitative health evaluation and disease state estimation by acceleration plethysmogram, Journal of Japan Society for Fuzzy Theory and Intelligent Informatics 15 (5) (2003) 565–576.
[21] S. Kwon, J. Hong, E.-K. Choi, E. Lee, D.E. Hostallero, W.J. Kang, B. Lee, E.-R. Jeong, B.-K. Koo, S. Oh, Y. Yi, Deep learning approaches to detect atrial fibrillation using photoplethysmographic signals: Algorithms development study, J. Med. Internet Res. 7 (6) (2019) e12770.
[22] E.M. Moreno, et al., Type 2 diabetes screening test by means of a pulse oximeter, I. E.E.E. Trans. Biomed. Eng. 64 (2) (2017) 341–351, https://doi.org/10.1109/TBME.2016.2554661.
[23] T. Saritas, et al., "Non-invasive evaluation of coronary heart disease in patients with chronic kidney disease using photoplethysmography,", Clin Kidney J 12 (4) (2019) 538–545, https://doi.org/10.1093/CKJ/SFY135.
[24] K. Kosasih, U.R. Abeyratne, V. Swarnkar, R. Triasih, Wavelet Augmented Cough Analysis for Rapid Childhood Pneumonia Diagnosis, I.E.E.E. Trans. Biomed. Eng. 62 (4) (2015) 1185–1194, https://doi.org/10.1109/TBME.2014.2381214.
[25] P. Porter *et al.*, "Diagnosing community-acquired pneumonia via a smartphone-based algorithm: a prospective cohort study in primary and acute-care consultations," *British Journal of General Practice*, vol. 71, no. 705, p. BJGP.2020.0750, Apr. 2020, 10.3399/bjgp.2020.0750.
[26] A. Imran, et al., AI4COVID-19: AI enabled preliminary diagnosis for COVID-19 from cough samples via an app, Inform Med Unlocked 20 (Jan. 2020) 100378, https://doi.org/10.1016/j.imu.2020.100378.
[27] H. Chen, X. Yuan, Z. Pei, M. Li, J. Li, Triple-Classification of Respiratory Sounds Using Optimized S-Transform and Deep Residual Networks, IEEE Access 7 (2019) 32845–32852, https://doi.org/10.1109/ACCESS.2019.2903859.
[28] E.D. McCollum, et al., Digital auscultation in PERCH: Associations with chest radiography and pneumonia mortality in children, Pediatr. Pulmonol. 55 (11) (2020) 3197–3208, https://doi.org/10.1002/ppul.25046.
[29] A. Rao, J. Ruiz, C. Bao, S. Roy, Tabla: A proof-of-concept auscultatory percussion device for low-cost pneumonia detection, Sensors (Switzerland) 18 (8) (2018), https://doi.org/10.3390/s18082689.
[30] K. Baker, T. Alfvén, A. Mucunguzi, A. Wharton-Smith, E. Dantzer, T. Habte, L. Matata, D. Nanyumba, M. Okwir, M. Posada, A. Sebsibe, J. Nicholson, M. Marasciulo, R. Izadnegahdar, M. Petzold, K. Källander, Performance of four respiratory rate counters to support community health workers to detect the symptoms of pneumonia in children in low resource settings: A prospective, multicentre, hospital-based, single-blinded, comparative trial, EClinicalMedicine 12 (2019) 20–30.

[31] W. Karlen, S. Raman, J.M. Ansermino, G.A. Dumont, Multiparameter respiratory rate estimation from the photoplethysmogram, I.E.E.E. Trans. Biomed. Eng. 60 (7) (2013) 1946–1953, https://doi.org/10.1109/TBME.2013.2246160.

[32] A. Capelastegui, et al., Validation of a predictive rule for the management of community-acquired pneumonia, Eur. Respir. J. 27 (1) (2006) 151–157, https://doi.org/10.1183/09031936.06.00062505.

[33] I. Amirav, M. Lavie, Rethink respiratory rate for diagnosing childhood pneumonia, EClinicalMedicine 12 (2019) 6–7.

[34] P. Modi, R.B. Mark Munyaneza, E. Goldberg, G. Choy, R. Shailam, P. Sagar, S. J. Westra, S. Nyakubyara, M. Gakwerere, V. Wolfman, A. Vinograd, M. Moore, A. C. Levine, Oxygen saturation can predict pediatric pneumonia in a resource-limited setting, J. Emerg. Med. 45 (5) (2013) 752–760.

[35] M.J. Lyu, S.M. Yuan, Cloud-based smart dog music therapy and pneumonia detection system for reducing the difficulty of caring for patients with dementia, IEEE Access 8 (2020) 20977–20990, https://doi.org/10.1109/ACCESS.2020.2969482.

[36] K. Mala, B. Manoj Kumar, R. Vignesh, and K. Manoj Kumar, "A wearable diagnostic device to combat children's pneumonia," in *GHTC 2016 - IEEE Global Humanitarian Technology Conference: Technology for the Benefit of Humanity, Conference Proceedings*, 2016. 10.1109/GHTC.2016.7857348.

[37] T. El Salti, E. R. Sykes, W. Zajac, S. Abdullah, and S. Khoja, "NewPneu: A Novel Cost Effective mHealth System for Diagnosing Childhood Pneumonia in Low-Resource Settings," in *2019 IEEE 10th Annual Information Technology, Electronics and Mobile Communication Conference, IEMCON 2019*, Institute of Electrical and Electronics Engineers Inc., Oct. 2019, pp. 5–12. 10.1109/IEMCON.2019.8936160.

[38] S. W. Chiu *et al.*, "A fully integrated nose-on-a-chip for rapid diagnosis of ventilator-associated pneumonia," *IEEE Trans Biomed Circuits Syst*, vol. 8, no. 6, pp. 765–778, Dec. 2014, 10.1109/TBCAS.2014.2377754.

[39] S. Doulou *et al.*, "A novel optical biosensor for the early diagnosis of sepsis and severe Covid-19: the PROUD study," *BMC Infect Dis*, vol. 20, no. 1, pp. 1–10, Dec. 2020, 10.1186/s12879-020-05607-1.

[40] "About Child & Teen BMI | Healthy Weight | DNPAO | CDC." https://www.cdc.gov/healthyweight/assessing/bmi/childrens_bmi/about_childrens_bmi.html (accessed Jan. 10, 2023).

[41] M. Elgendi, "Optimal signal quality index for photoplethysmogram signals,", Bioengineering 3 (4) (2016) https://doi.org/10.3390/BIOENGINEERING3040021.

[42] X. Zhang, Y. Lyu, T. Qu, P. Qiu, X. Luo, J. Zhang, S. Fan, Y. Shi, Photoplethysmogram-based cognitive load assessment using multi-feature fusion model, ACM Trans. Appl. Percept. 16 (4) (2019) 1–17.

[43] H. Demirtas and B. Doganay, "Simultaneous Generation of Binary and Normal Data with Specified Marginal and Association Structures," *https://doi.org/10.1080/10543406.2010.521874*, vol. 22, no. 2, pp. 223–236, Mar. 2012, 10.1080/10543406.2010.521874.

[44] "Anderson–Darling Test," *The Concise Encyclopedia of Statistics*, pp. 12–14, Feb. 2008, 10.1007/978-0-387-32833-1_11.

[45] E. Whitley, J. Ball, Statistics review 6: Nonparametric methods, Crit. Care 6 (6) (Dec. 2002) 509, https://doi.org/10.1186/CC1820.

[46] W. Haynes, "Wilcoxon Rank Sum Test," *Encyclopedia of Systems Biology*, pp. 2354–2355, 2013, 10.1007/978-1-4419-9863-7_1185.

[47] "An Industrial IoT Approach for Pharmaceutical Industry Growth | ScienceDirect." https://www.sciencedirect.com/book/9780128213261/an-industrial-iot-approach-for-pharmaceutical-industry-growth (accessed Mar. 07, 2023).

[48] T. Nguyen, M. Raghu, and S. Kornblith, "Do Wide and Deep Networks Learn the Same Things? Uncovering How Neural Network Representations Vary with Width and Depth," Oct. 2020, 10.48550/arxiv.2010.15327.

[49] "What is Bagging? | IBM." https://www.ibm.com/topics/bagging (accessed Mar. 08, 2023).

[50] M. Radovic, M. Ghalwash, N. Filipovic, Z. Obradovic, Minimum redundancy maximum relevance feature selection approach for temporal gene expression data, BMC Bioinf. 18 (1) (2017) 1–14, https://doi.org/10.1186/S12859-016-1423-9/FIGURES/6.

[51] T. Iqbal, A. Elahi, S. Ganly, W. Wijns, A. Shahzad, Photoplethysmography-based respiratory rate estimation algorithm for health monitoring applications, J Med Biol Eng 42 (2) (2022) 242, https://doi.org/10.1007/S40846-022-00700-Z.

[52] K. Selvakumar, et al., Realtime PPG based respiration rate estimation for remote health monitoring applications, Biomed. Signal Process. Control 77 (2022) 103746, https://doi.org/10.1016/J.BSPC.2022.103746.

[53] A. Rao, J. Ruiz, C. Bao, S. Roy, Tabla: A proof-of-concept auscultatory percussion device for low-cost pneumonia detection, Sensors 18 (8) (2018) 2689, https://doi.org/10.3390/s18082689.

[54] P. Özen Kavas, M. Recep Bozkurt, İ. Kocayiğit, C. Bilgin, "Machine learning-based medical decision support system for diagnosing HFpEF and HFrEF using PPG,", Biomed Signal Process Control 79 (2023) 104164, https://doi.org/10.1016/J.BSPC.2022.104164.

[55] F. Riaz, M.A. Azad, J. Arshad, M. Imran, A. Hassan, S. Rehman, Pervasive blood pressure monitoring using Photoplethysmogram (PPG) sensor, Futur. Gener. Comput. Syst. 98 (2019) 120–130, https://doi.org/10.1016/J.FUTURE.2019.02.032.

[56] S.G. Khalid, S.M. Ali, H. Liu, A.G. Qurashi, U. Ali, Photoplethysmography temporal marker-based machine learning classifier for anesthesia drug detection, Med. Biol. Eng. Compu. 60 (11) (2022) 3057–3068, https://doi.org/10.1007/S11517-022-02658-1/TABLES/3.

[57] M.X. Xiao, C.H. Lu, N. Ta, H.C. Wei, C.C. Yang, H.T. Wu, Toe PPG sample extension for supervised machine learning approaches to simultaneously predict type 2 diabetes and peripheral neuropathy, Biomed. Signal Process. Control 71 (2022) 103236, https://doi.org/10.1016/J.BSPC.2021.103236.

[58] S. El-Sappagh, F. Ali, T. Abuhmed, J. Singh, J.M. Alonso, Automatic detection of Alzheimer's disease progression: An efficient information fusion approach with heterogeneous ensemble classifiers, Neurocomputing 512 (2022) 203–224, https://doi.org/10.1016/J.NEUCOM.2022.09.009.

[59] A.H. Syed, T. Khan, A. Hassan, N.A. Alromema, M. Binsawad, A.O. Alsayed, An ensemble-learning based application to predict the earlier stages of alzheimer's disease (AD), IEEE Access 8 (2020) 222126–222143, https://doi.org/10.1109/ACCESS.2020.3043715.

[60] S.G. Shaikh, B. SureshKumar, G. Narang, "Development of optimized ensemble classifier for dengue fever prediction and recommendation system,", Biomed Signal Process Control 85 (2023) 104809, https://doi.org/10.1016/J.BSPC.2023.104809.

[61] D. Castaneda, A. Esparza, M. Ghamari, C. Soltanpur, H. Nazeran, "A review on wearable photoplethysmography sensors and their potential future applications in health care,", Int J Biosens Bioelectron 4 (4) (2018) 195, https://doi.org/10.15406/IJBSBE.2018.04.00125.

[62] M. Nazeer, M. Qayyum, and A. Ahad, "Real Time Object Detection And Recognition In Machine Learning Using Jetson Nano." Nov. 03, 2022. Accessed: Jun. 20, 2023. [Online]. Available: https://papers.ssrn.com/abstract=4286087.

[63] "Jetson Nano Developer Kit | NVIDIA Developer." https://developer.nvidia.com/embedded/jetson-nano-developer-kit (accessed Jun. 20, 2023).

[64] H.W. Loh, et al., Application of photoplethysmography signals for healthcare systems: An in-depth review, Computer Methods and Programs in Biomedicine 216 (2022) 106677, https://doi.org/10.1016/J.CMPB.2022.106677.

[65] S. Maqsood, et al., A survey: From shallow to deep machine learning approaches for blood pressure estimation using biosensors, Expert Syst. Appl. 197 (2022) 116788, https://doi.org/10.1016/J.ESWA.2022.116788.

[66] M. Elgendi, R.R. Fletcher, H. Tomar, J. Allen, R. Ward, C. Menon, The striking need for age diverse pulse oximeter databases, Front Med (Lausanne) 8 (2021), https://doi.org/10.3389/FMED.2021.782422.

[67] S.G. Khalid, J. Zhang, F. Chen, D. Zheng, Blood pressure estimation using photoplethysmography only: comparison between different machine learning approaches, J Healthc Eng 2018 (2018), https://doi.org/10.1155/2018/1548647.

[68] Y. Liang, Z. Chen, G. Liu, M. Elgendi, "A new, short-recorded photoplethysmogram dataset for blood pressure monitoring in China,", Sci. Data 5 (1) (2018) https://doi.org/10.1038/sdata.2018.20.

[69] N. Nirala, R. Periyasamy, B.K. Singh, A. Kumar, Detection of type-2 diabetes using characteristics of toe photoplethysmogram by applying support vector machine, Biocybern Biomed Eng 39 (1) (2019) 38–51, https://doi.org/10.1016/j.bbe.2018.09.007.

[70] S. Shimawaki, Y. Kobayashi, M. Nakabayashi, N. Sakai, Non-invasive serum cholesterol detection using near-infrared light transmission, Biomedical Engineering Research Sept. 3 (3) (2014) 80–87, https://doi.org/10.5963/ber0303003.

[71] F.M. rukam Muharni, "Review on non invasive glucose and cholesterol measurement system,", IOP Conf Ser Mater Sci Eng 590 (1) (2019) 012030, https://doi.org/10.1088/1757-899X/590/1/012030.

[72] Y. Li, H. Gao, Y. Ma, "Evaluation of pulse oximeter derived photoplethysmographic signals for obstructive sleep apnea diagnosis,", Medicine (United States) 96 (18) (2017) https://doi.org/10.1097/MD.0000000000006755.

[73] J.U. Park, H.K. Lee, J. Lee, E. Urtnasan, H. Kim, K.J. Lee, Automatic classification of apnea/hypopnea events through sleep/wake states and severity of SDB from a pulse oximeter, Physiol. Meas. 36 (9) (2015) 2009–2025, https://doi.org/10.1088/0967-3334/36/9/2009.

[74] N. Paradkar and S. R. Chowdhury, "Cardiac arrhythmia detection using photoplethysmography," in *Proceedings of the Annual International Conference of the IEEE Engineering in Medicine and Biology Society, EMBS*, Institute of Electrical and Electronics Engineers Inc., Sep. 2017, pp. 113–116. 10.1109/EMBC.2017.8036775.